AN ABSTRACT OF THE DISSERTATION OF

Thomas Schumacher for the degree of Doctor of Philosophy in Civil Engineering presented on November 20, 2009.

Title: New Acoustic Emission Applications in Civil Engineering

Abstract approved:

Christopher C. Higgins

Non-destructive testing methods and applications have become of increasing interest due to the worldwide aging and deteriorating infrastructure network. In the field of Civil Engineering, bridges and bridge components as well as non-structural elements such as roadway pavements for example, are affected. In particular, the Acoustic Emission (AE) technique offers the unique opportunity to monitor infrastructure components in real-time and detect sudden changes in the integrity of the monitored element. The principle is that dynamic input sources cause a stress wave to form, travel through the body, and create a transient surface displacement that can be recorded by piezo-electric sensors located on the surface. Commonly, analysis methods of purely qualitative nature are used to estimate the current condition or make predictions on the future state of a monitored component. Using quantitative analysis methods, source locations and characteristics can be deduced, similarly to the case for earthquake sources. If properly configured, crack formation and propagation can hence be quantified with this technique. The research work presented in this dissertation, however, goes past commonly found AE applications. Three novel applications have been developed: (1) a new prospective detection tool was discovered in the field of Transportation Engineering where AE sensors were employed to identify vehicles equipped with studded tires passing over bridges. Such vehicles cause costly damage each year to the roadway infrastructure network and this tool would enable gathering statistical data or enforcing legal dates for the use of studded tires. Load conditions of two full-scale laboratory bridge girders were estimated analyzing AE data collected from applied service-level loads using an earthquake prediction method called *b*-value analysis (2). It was found that this analysis method may assist in estimating the operating load conditions of in-service bridges. Finally (3), a novel framework for the development of a probabilistic stress wave source location

algorithm based on Bayesian analysis methods is proposed. Markov Chain Monte Carlo simulation was employed to estimate model parameters and predict source locations in full probabilistic form. Because variability in the materials and errors in the model can be included, a more accurate solution is available.

New Acoustic Emission Applications in Civil Engineering

by
Thomas Schumacher

A DISSERTATION

submitted to

Oregon State University

in partial fulfillment of
the requirements for the
degree of

Doctor of Philosophy

Presented November 20, 2009
Commencement June 2010

Doctor of Philosophy dissertation of Thomas Schumacher presented on November 20, 2009.

APPROVED:

Major Professor, representing Civil Engineering

Head of the School of Civil and Construction Engineering

Dean of the Graduate School

I understand that my dissertation will become part of the permanent collection of Oregon State University libraries. My signature below authorizes release of my dissertation to any reader upon request.

Thomas Schumacher, Author

ACKNOWLEDGEMENTS

First and foremost, I want to express my sincere appreciation to my adviser Dr. Christopher Higgins for his unquestioning support during my endeavor to earning a doctoral degree. His immense knowledge of just about anything in structural engineering added a great deal to my success. Dr. Higgins' sometimes surprising and unpredictable technical as well as philosophical questions (related and/or unrelated to what I was working on) were always very stimulating and helped tremendously improve my thought process and work.

Dr. Steven Lovejoy from the Oregon Department of Transportation assisted in data collection and analysis. In addition, he invited me along to several bridge instrumentation installations which provided me first-hand inspection experience and exposed me to the challenges therein. On top of that, the trips were always fun and I thank him for the good times and the friendship.

Dr. Daniel Straub introduced me to Bayesian Statistics and advised on the implementation and interpretation of an analytical framework that was completely new to me. Thanks to him, I am 95% confident that there is a 0.90 probability that I know a little bit more about Bayesian Statistics than the average person. I think.

I also want to thank Dr. Steven Glaser and Dr. Christian Grosse. It has been a great honor and pleasure to collaborate with and learn from these two top experts in the field of non-destructive testing and monitoring. They were always open and available at any time for my questions.

I also want to thank all my colleagues and friends that have accompanied me during my stay here in Corvallis. I will never forget the companionship I experienced in this research group.

Dr. Brian Bay, Dr. Michael Scott, Dr. Daniel Cox, and Dr. Philip Humphrey served in my PhD committee and their questions and comments are appreciated.

Finally, I want thank my parents Hanni and Willi, to which this dissertation is dedicated, and my girlfriend Kelsea for their loving moral support. The complaining and whining about the challenges of a PhD shall be over. I thank you for listening to and enduring it.

CONTRIBUTION OF AUTHORS

Dr. Christopher C. Higgins advised on data collection, analysis and interpretation of Chapters 2, 3, and 4. Dr. Steven C. Lovejoy assisted in data collection and interpretation of Chapters 2 and 3. Dr. Daniel Straub advised on the conceptual framework and assisted in data analysis and interpretation of Chapter 3.

TABLE OF CONTENTS

Page

TABLE OF CONTENTS (Continued)

Page

TABLE OF CONTENTS (Continued)

Page

LIST OF FIGURES

Figure Page

LIST OF FIGURES (Continued)

Figure Page

LIST OF TABLES

WIDMUNG (DEDICATION)

Ich widme diese Doktorarbeit meinen Eltern, Hanni und Willi Schumacher. Ich danke Euch für alles, was Ihr mir auf meinem Lebensweg mitgegeben habt. Ohne Eure stetige moralische Unterstützung und den Glauben an mich und meine Fähigkeiten hätte ich es nie soweit gebracht.

1 General Introduction

1.1 Background and Introduction

Non-destructive testing methods and applications have become of increasing interest due to the worldwide aging and deteriorating infrastructure network (Colombo et al. 2003a; Glaser 2004; Grosse et al. 2006; Lovejoy 2006; Ohtsu 1996; Uomoto 1987). In the field of Civil Engineering, bridges and bridge components as well as non-structural elements such as roadway pavements for example, are affected. In particular, the Acoustic Emission (AE) technique offers the unique opportunity to monitor infrastructure components in real-time and detect sudden changes in the integrity of the monitored element (Grosse and Ohtsu 2008). Networks of piezo-electric sensors are used that respond to surface displacements caused by propagating stress waves (Miller et al. 2005). Fig. 1.1 shows a typical sensor network, including eight sensors, for experimental testing of a full-scale reinforced concrete (RC) bridge girder (Schumacher 2008). There are also sensors mounted to the back face of this test specimen that are not visible in the image.

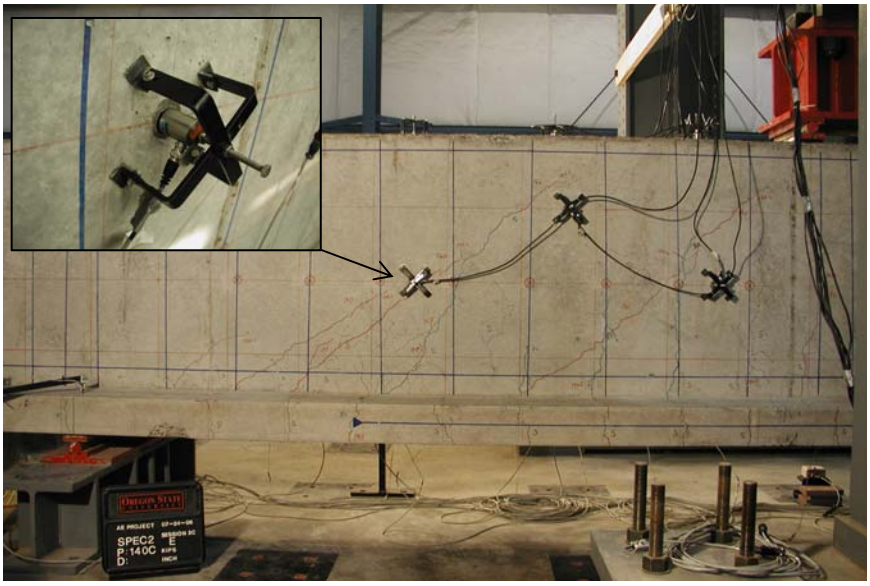

Fig. 1.1–AE sensor network used for experimental testing, one sensor with fixture shown enlarged

Acoustic Emission (AE) is the *term used for transient elastic waves generated by the release of energy within a material or by a process* (EN 2000). A stress wave is generated, traveling from the source origin away to the surface of the body where it can be recorded by sensors. This process is irreversible and therefore not repeatable. Other terms include stress wave emission or

nano-seismic activity. Within the family of non-destructive testing methods, AE has its own special place because it is a passive technique. AE are stress waves produced by a spontaneous internal dynamic process such as crack initiation or formation or internal material fracture. The source location and mechanism is therefore unknown and subject to investigation. In this dissertation, the terms Acoustic Emission (or AE) and stress wave are used interchangeably.

The principle of the AE method is that dynamic input sources cause a stress wave to form, travel through the body, and create a transient surface displacement are recorded by the sensors, provided the signal is strong enough to be detected. AE sensors typically consist of a piezo-electric crystal that creates a voltage output that is proportional to the imposed strain caused by a transient surface displacement. This signal is then intensified by a pre-amplifier. Usually not only one but several sensors are deployed to record data in parallel. In order to store data on the hard disk, the analog sensor signals must first be digitized by an A/D-converter. Typically, data are not acquired continuously since that would generate enormous data files which would be hard to interpret. Instead, pre-selected criteria are used to trigger the recording system for individual AE burst signals from which descriptive parameters and wave form traces are then extracted. All this is done in real-time and requires a powerful data acquisition system. For a three-dimensional array like the one shown in Fig. 1.1, it is possible to estimate the location of the source based on arrival time differences, very similar to the case of earthquakes (Ge 2003a; Ge 2003b; Geiger 1910; Grosse et al. 1997). If properly configured, crack formation and propagation can hence be tracked with this technique. Many analysis methods were actually adapted from seismic applications due to the similar natures of the problems. Fig. 1.2 shows a typical AE wave form an experiment on a full-scale RC beam. Frequencies range from approximately 10 to 500 kHz.

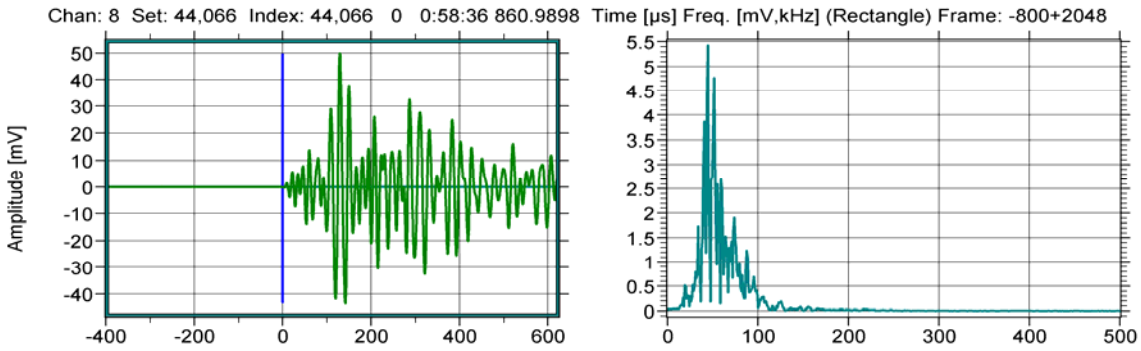

Fig. 1.2–Typical AE wave form from RC applications

The fact that material under plastic deformation or when cracking emits audible sounds has been known for centuries (Miller et al. 2005). Early investigations were qualitative in nature and restricted to the frequency range of the human ear. The necessary tools to measure and record such sounds were finally developed in the early 20th century.

Joseph Kaiser from the University in Munich, Germany is considered the pioneer in modern AE research. In 1950, he published his findings of AE measurements during tension tests on metals (Kaiser 1950). The Kaiser Effect states that sounds are emitted from a material only when a previously experienced stress level is exceeded. Fowler et al. discovered in the 1960s that this is not always true for composite materials (Fowler et al. 1989). This phenomenon was named Felicity Ratio. One of the first documented AE tests on reinforced concrete was conducted at the University of Washington to investigate debonding of embedded reinforcing steel from cyclic loading of a beam-column connection (Kobayashi et al. 1980). After that, AE monitoring has increasingly been utilized to investigate fracture processes and to characterize damage of RC elements (Colombo et al. 2003b; Köppel and Vogel 2000; Lovejoy 2008; Ohtsu et al. 2002; Schechinger 2006; Shiotani et al. 2000; Uomoto 1987).

AE research can generally be divided in two major categories: Qualitative vs. quantitative AE analysis methods (Grosse 1996; Köppel 2002). Qualitative methods appear to work for defined problems where the boundary conditions (size, geometry, material properties, crack pattern, sensor array, etc.) do not significantly change over time. Only a few key parameters, which are assumed to characteristically describe an AE signal wave form, are extracted and stored for later interpretation. For large structures with a number of different potential sources such as full-scale RC members, they can only give a rough qualitative and relative overview of the internal processes. Quantitative methods try to describe the nature of a source by using for example moment tensor inversion (MTI) techniques (Grosse et al. 2003; Köppel 2002; Ohtsu et al. 1998). However, a MTI is not always easy to perform, especially for large structures and when using a small number of sensors. Just recently, the first full-scale experiments on RC beams were successfully conducted using MTI methods (Katsaga et al. 2007). Quantitative methods are probably the most accurate and physically meaningful means to describe fracture processes within a structural element, but much work is still needed before this method is ready for the field.

One notable challenge in AE testing is the discrimination of spurious sources that are not of interest to the problem but can skew or interfere with data analysis. This is especially difficult for complex materials such as RC which is a composite material consisting of fine and coarse aggregates, cement, and reinforcing steel. All of these components have different dynamic material properties and damping characteristics. Additionally, RC components usually crack under service conditions, causing changing boundary conditions for the stress waves.

1.2 Scope and Layout of this Dissertation

This PhD dissertation follows the manuscript option as described in the OSU Graduate School Thesis Guide 2009-2010 and covers a series of innovative AE applications in Civil Engineering. Three technical papers with original content were developed and are introduced below. They will undoubtedly help address urgent problems in monitoring and maintaining crucial parts of the infrastructure transportation network. The first two represent novel real-world application tools that can be used for monitoring; the third embodies a new methodology for a common problem in AE. This dissertation is structured as follows:

Chapter 1: *General Introduction*.

Chapter 2: *Manuscript 1*. The title of this first technical paper is "Detection of Vehicles with Studded Tires Using Acoustic Emission Sensors Mounted to Highway Bridges." Studded tires have caused hundreds of millions of dollars worth of damage to highway pavements alone in the Pacific Northwest. Studded tire use causes increased pavement wear and creates rutting which can lead to other safety problems such as hydroplaning, for example. AE offers a potential tool to detect passing vehicles that are equipped with studded tires. Past studies on the use of studded tires have highlighted the need for a tool to better estimate the number of vehicles with studded tires that travel a road network. Currently, there is no such tool available. This manuscript presents a detection methodology using AE techniques to identify vehicles operating with studded tires. Data from an in-service test on a highway bridge were utilized for developing and evaluating two proposed detection schemes. It was found that using relatively simple detection algorithms, vehicles with studded tires could reliably be discriminated. A practicable integrated system is proposed as that could be implemented for detection and monitoring of studded snow tire use on highway systems. This manuscript was submitted to the *ASCE Journal of Transportation Engineering* and accepted for publication on April 4, 2009.

Chapter 3: *Manuscript 2*. This second technical paper is titled "Estimating Operating Load Conditions on Reinforced Concrete Highway Bridges with b-Value Analysis from Acoustic Emission Monitoring." Transportation agencies commonly have conventionally steel reinforced concrete deck girder (RCDG) bridges in their inventory that were built in the mid-twentieth century. These bridges have been in-service beyond their intended design lives and tools are

needed to permit freight mobility and maintain operational safety. The practical applicability of AE monitoring techniques were investigated to help estimate the operating condition of diagonally cracked RCDG bridges. Experiments on two full-scale girder specimens representative of Oregon's RCDG bridges were built and tested under realistic service conditions. Overloading conditions were imposed to increase the level of deterioration. It was found that characterizing the current health condition of a monitored bridge component or element based on short term in-service loading is difficult and the proximity of a potential bridge failure not easily predictable until it is impending. However, it was observed that the current operating load level of a bridge component can be estimated using a newly proposed method called *Minimum b-Value Analysis*. By performing such an analysis, it can be estimated whether the applied truck load is comparable to loads that the bridge has been experiencing, or whether they are higher or lower. The influence of factors that can affect *b*-value estimations such as stage of deterioration or external sources was studied and is presented. The experiment as well as data from the two laboratory specimens are evaluated. This manuscript was submitted to the journal of *Structural Health Monitoring* and accepted for publication on October 5, 2009.

Chapter 4: *Manuscript 3*. The title of this third and last technical paper is "Estimation of Acoustic Emission Source Locations: A Bayesian Approach." Acoustic Emissions (AE) are stress waves initiated by sudden strain releases within a solid body. These can be caused by internal mechanisms such as crack opening or propagation, crushing, or rubbing of crack surfaces. One application for the AE technique in the field of Structural Engineering is Structural Health Monitoring (SHM). With piezo-electric sensors mounted to the surface of the structure, stress waves can be detected, recorded, and stored for later analysis. An important step in quantitative AE analysis is the estimation of the stress wave source location. Commonly, source location results are presented in a purely deterministic manner as spatial and temporal points, excluding information about uncertainties and errors. Due to variability in the material properties and uncertainty in the mathematical model, measures of uncertainty are needed beyond best-fit point solutions for source locations. This paper introduces a framework for the development of a probabilistic source location algorithm using Bayesian analysis methods with Markov Chain Monte Carlo (MCMC) simulation where all source location parameters are described with a posterior probability density function (PDF). The proposed methodology is applied to an example employing data collected from a realistic section of a reinforced concrete bridge column. The

selected approach is general and has the advantage that it can be extended and refined efficiently. Results are discussed and future steps to improve the algorithm suggested. This manuscript will be submitted to the *Journal of Sound and Vibration*.

Chapter 5: *General Conclusion*.

1.3 References

Colombo, S., Forde, M. C., Main, I. G., and Halliday, J. (2003a). "AE monitoring of concrete bridge beams in situ." *The Structural Engineer*, 81(23), 41-46.

Colombo, S., Main, I. G., and Forde, M. C. (2003b). "Assessing Damage of Reinforced Concrete Beam Using "b-value" Analysis of Acoustic Emission Signals." *ASCE Journal of Materials in Civil Engineering*, 15(3), 280-286.

EN. (2000). "1330-9: Non-destructive testing-Terminology-Part 9: Terms used in acoustic emission testing." European Committee for Standardization (CEN), Brüssel, Belgium.

Fowler, T. J., Blessing, J. A., and Conlisk, P. J. (1989). "New Directions in Testing." Third International Symposium on Acoustic Emission from Composite Materials AECM-3, Paris, France, 16-27.

Ge, M. (2003a). "Analysis of Source Location Algorithms, Part I: Overview and non-iterative methods." *Journal of Acoustic Emission*, 21, 14-28.

Ge, M. (2003b). "Analysis of Source Location Algorithms, Part II: Iterative methods." *Journal of Acoustic Emission*, 21, 29-51.

Geiger, L. (1910). "Herdbestimmung bei Erdbeben aus den Ankunftszeiten." *Nachrichten von der Königlichen Gesellschaft der Wissenschaften zu Göttingen*, 4, 331-349.

Glaser, S. D. (2004). "Some Real-World Applications of Wireless Sensor Nodes." SPIE Smart Structures and Materials 2004, San Diego, CA, 344-355.

Grosse, C. U. (1996). "Quantitative zerstörungsfreie Prüfung von Baustoffen mittels Schallemissionsanalyse und Ultraschall," PhD Dissertation, University of Stuttgart, Stuttgart, Germany.

Grosse, C. U., Glaser, S. D., and Krüger, M. (2006). "Condition Monitoring of Concrete Structures Using Wireless Sensor Networks and MEMS." SPIE Smart Structures and Materials: Sensors and Smart Structures Technology for Civil, Mechanical, and Aerospace Systems, 407-418.

Grosse, C. U., and Ohtsu, M. (2008). *Acoustic Emission Testing - Basics for Research-Applications in Civil Engineering*, Springer Verlag, Berlin & Heidelberg, Germany.

Grosse, C. U., Reinhardt, H.-W., and Dahm, T. (1997). "Localization and classification of fracture types in concrete with quantitative acoustic emission measurement techniques." *NDT & E International*, 30(4), 223-230.

Grosse, C. U., Reinhardt, H.-W., and Finck, F. (2003). "Signal-Based Acoustic Emission Techniques." *ASCE Journal of Materials in Civil Engineering*, 15(3), 274-279.

Kaiser, J. (1950). "Untersuchungen über das Auftreten von Geräuschen beim Zugversuch," PhD Dissertation, Technische Universität München, Munich, Germany.

Katsaga, T., Sherwood, E. G., Collins, M. P., and Young, R. P. (2007). "Acoustic emission imaging of shear failure in large reinforced concrete structures." *International Journal of Fracture*, 148(1), 29-45.

Kobayashi, A. S., Hawkings, N. M., Chan, Y.-L., and Lin, I.-J. (1980). "A Feasibility Study of Detecting Reinforcing-Bar Debonding by Acoustic-emission Technique." *Experimental Mechanics*, 20(9), 301-308.

Köppel, S. (2002). "Schallemissionsanalyse zur Untersuchung von Stahlbetontragwerken," PhD Dissertation, Eidgenössische Technische Hochschule Zürich, Zurich, Switzerland.

Köppel, S., and Vogel, T. (2000). "Schallemissionsmessungen bei Versuchen an Stahlbeton." Institut für Baustatik und Konstruktion, Zurich, Switzerland.

Lovejoy, S. C. (2006). "Development of Acoustic Emissions Testing Procedures Applicable to Convetionally Reinforced Concrete Deck Girder Bridges Subjected to Diagonal Tension Cracking," PhD Dissertation, Oregon State University, Corvallis, OR.

Lovejoy, S. C. (2008). "Acoustic Emission Testing of Beams to Simulate SHM of Vintage Reinforced Concrete Deck Girder Highway Bridges." *Structural Health Monitoring*, 7(4), 329-346.

Miller, R. K., Hill, E. v. K., and Moore, P. O. (2005). *Nondestructive Testing Handbook - Volume 6 - Acoustic Emission Testing*, American Society for Nondestructive Testing (ASNT), Columbus, OH.

Ohtsu, M. (1996). "The history and development of acoustic emission in concrete engineering." *Magazine of Concrete Research*, 48(177), 321-330.

Ohtsu, M., Okamoto, T., and Yuyama, S. (1998). "Moment Tensor Analysis of Acoustie Emission for Cracking Mechanisms in Concrete." *ACI Structural Journal*, 95(2), 87-95.

Ohtsu, M., Uchida, M., Okamoto, T., and Yuyama, S. (2002). "Damage Assessment of Reinforced Concrete Beams Qualified by Acoustic Emission." *ACI Structural Journal*, 99(4), 411-417.

Schechinger, B. (2006). "Schallemissionsanalyse zur Ueberwachung der Schädigung von Stahlbeton," PhD Dissertation, Eidgenössische Technische Hochschule Zürich, Zurich, Switzerland.

Schumacher, T. (2008). "Acoustic Emission Techniques Applied to Conventionally Reinforced Concrete Bridge Girders." Oregon Department of Transportation (ODOT), Salem, OR.

Shiotani, T., Yuyama, S., Li, Z. W., and Ohtsu, M. (2000). "Quantitative Evaluation of Fracture Processes in Concrete by the Use of Improved b-Value." Non-Destructive Testing in Civil Engineering 2000 (Seiken Symposium No. 26), Elsevier, Tokyo, Japan, 293-302.

Uomoto, T. (1987). "Application of Acoustic Emission to the Field of Concrete Engineering." *Journal of Acoustic Emission*, 6(3), 137-144.

Detection of Vehicles with Studded Tires Using Acoustic Emission Sensors Mounted to Highway Bridges

Thomas Schumacher, Christopher C. Higgins, and Steven C. Lovejoy

ASCE Journal of Transportation Engineering
ASCE Publications
1801 Alexander Bell Dr
Reston, VA 20191
USA

Accepted for publication on April 4, 2009

2 First Manuscript

Detection of Vehicles with Studded Tires Using Acoustic Emission Sensors Mounted to Highway Bridges

Thomas Schumacher[1], Christopher C. Higgins[2], and Steven C. Lovejoy[3]

Abstract: Transportation agencies expend large amounts of money annually to maintain highway wearing surfaces. Wear depends mainly on axle weight, vehicle speed, temperature, surface type, and the type of tires mounted on vehicles. When studded tires are used, wear is increased significantly. Past studies on the use of studded tires have highlighted the need for a tool to better estimate the number of vehicles with studded tires that travel a road network. Currently, there is no such tool available. This paper presents a detection methodology using Acoustic Emission techniques to identify vehicles operating with studded tires. Data from an in-service test on a highway bridge were utilized for developing and evaluating two proposed detection schemes. It was found that using relatively simple detection algorithms, vehicles with studded tires could be discriminated reliably. Finally, a practicable integrated system is proposed that could be implemented for detection and monitoring of studded snow tire use on highway systems.

Keywords: Studded tires, Acoustic Emission Monitoring, Real-time detection, Highway bridges.

[1] Graduate Research Assistant, School of Civil and Construction Engineering, Oregon State University, USA; E-mail: schumact@engr.orst.edu

[2] Professor, School of Civil and Construction Engineering, Oregon State University, USA; E-mail: chris.higgins@oregonstate.edu

[3] Senior Research Engineer, Oregon Department of Transportation, Bridge Engineering Section, Salem, OR, USA; E-mail: steven.c.lovejoy@odot.state.or.us

2.1 Introduction

Transportation agencies expend large amounts of money annually to repair and replace highway wearing surfaces. A study by Brunette and Lundy (1996) estimated that total damage for 1994 due to studded tires in the State of Oregon's road network was about $70 million. A more recent study by Malik (2000) estimated expenditures for repairing studded tire damage from 1994 to 2005 to total of about $103 million for the Oregon highway system alone. This estimate assumes average pavement design life and wear rate. The total number of vehicles with studded tires was estimated based on parking lot counting and telephone surveys. A more recent study was published by Zubeck et al. (2004) and covers the socio-economic impact of studded tire use in Alaska. It was concluded that the use of studded tires in Alaska may actually have a positive impact on the Alaskan economy. The savings from avoided accidents were the most substantial benefit. However, relation between rutted pavements and summer hydroplaning accidents was not taken into account. Here as well, visual inspection and vehicle counting on parking lots was used to determine the stud usage rate. The most recent data published by the Washington State Department of Transportation (WSDOT 2006) has revealed that damage from the use of studded tires on Portland cement concrete highways alone resulted approximately $18 million of additional cost within the state of Washington, with damage for asphalt concrete much higher.

Currently, no automated tools are available to accurately identify the number of vehicles with studded tires traveling on a highway network. It would be of great interest to estimate the number of vehicles with studded tires that operate after the legal dates. Enforcing these dates could be a first start to reduce damage on the infrastructure. Presented in this paper is the development and evaluation of detection methods based on the Acoustic Emission (AE) technique. An integrated system that enables automated real-time detection of vehicles with studded tires is proposed. This tool could be employed to establish statistics about the use of studded tires and could further be used as an enforcement tool to identify studded tire use past the allowable use date.

2.2 Background

2.2.1 Problems Associated with the Use of Studded Tires

Studded tires are winter tires that are equipped with studs made of metal or plastic materials designed to improve traction for winter driving. The studs protrude from the tire surface and are usually made of Tungsten Carbide, a very high strength metal. They are held in place by metal jackets inserted in the tire. Detailed information about studded tires, damage mechanisms to wearing surfaces, and state regulations can be found in a study published by the Washington State Transportation Center (Angerinos et al. 1999). For the State of Oregon, Brunette and Lundy (1996) estimated the wear rate on asphalt concrete and Portland cement concrete to be about 0.86 and 0.20 mm (0.034 and 0.008 in.) per 100,000 studded tires passes, respectively.

While benefits have been identified for users, problems have arisen with the use of studded tires including:

1. Ruts are produced in rigid (Portland cement concrete) as well as flexible (asphalt concrete) pavements that fill with water and ice and can cause hydroplaning and slipping
2. May polish aggregates and reduce friction
3. May make driving more difficult during dry conditions
4. Loosened wearing surface particles become airborne dust and contribute to air pollution
5. Increased noise level
6. On dry and wet surfaces (no ice), regular winter tires have better traction than studded tires

In most states where studded tires are allowed, there are date restrictions on when it is legal to drive with studded tires. Wyoming, Colorado, and New Mexico allow the use of studded tires without restrictions. Unfortunately, there are no data available on the damage caused by studded tires in these states. In Oregon, tires equipped with lightweight studs are legal between November 30 and April 3. In the State of Washington, it is November 1 to March 31. Motorists are encouraged to use studded tires only when necessary because of the increased damage they cause to roadways; however few dismount and remount studded tires during the permissible season.

2.2.2 Acoustic Emission Monitoring

Acoustic Emissions (AE) are the result of a sudden, spontaneous strain release within a solid body, i.e. the formation of a crack. A stress wave is generated, traveling from the source origin away to the surface of the body where it can be detected by sensors. Other names for AE include stress wave emission or micro-seismic activity (Miller et al. 2005). Formally defined, AE is the *term used for transient elastic waves generated by the release of energy within a material or by a process* (EN 2000). The AE technique has been established as a means to monitor structural deterioration, e.g. material fracture, and has hence found applications in material science and structural health monitoring, e.g. of bridges.

The general principle of AE data acquisition is that emitted stress waves are recorded, stored, and then analyzed. Piezo-electric based sensors mounted to the surface of the test object are typically used for AE monitoring, which produce a voltage-versus-time signal from the dynamic surface motion (Miller et al. 2005). A thin layer of high vacuum grease is typically used as a couplant between sensor and concrete surface. The generated voltage signal output is proportional to the surface pressure and dependent on the size and damping characteristics of the sensor. Ideally, a sensor should have a very flat response over the whole frequency range. This is necessary for wave form analyses, but sensors of this kind tend to be not very sensitive which makes it difficult to detect AE signals in reinforced concrete (RC) at a distance of more than a few meters. Resonant sensors are sensitive at their resonant frequency and have proven to work well for AE signal detection in RC (Lovejoy 2006; Schumacher 2008). This signal is then intensified by a pre-amplifier. Usually not only one but several sensors are deployed and record data in parallel. In order to store data on the hard disk, the analog sensor signals must first be digitalized. Typically, AE data is not acquired continuously, since that would yield enormous data files which would be hard to interpret. Pre-selected criteria are used to trigger the system for individual AE burst signals from which descriptive parameters and wave forms are then extracted. For this study, the most important parameter was AE hit amplitude, which is the maximum voltage measured during a discriminated AE burst signal and represented on a decibel scale. All this is done in real-time and requires a powerful data acquisition system.

Fig. 2.1 schematically illustrates the elements of a typical AE data acquisition system. In this case, the stress wave is released from within the body. For the case of studded tires, the source is

introduced on one side of the body, then travels through it and is eventually detected by the sensor on the opposite side of the body.

In structural health monitoring, a source such as the discussed one caused by studded tires would be considered as noise as it is generated from an external artificial source which should be filtered out as it can significantly bias damage detection algorithms. For this study, however, it becomes the source of main interest. As will be shown in this paper, it is fairly uncomplicated to detect vehicles with studded tires with high reliability.

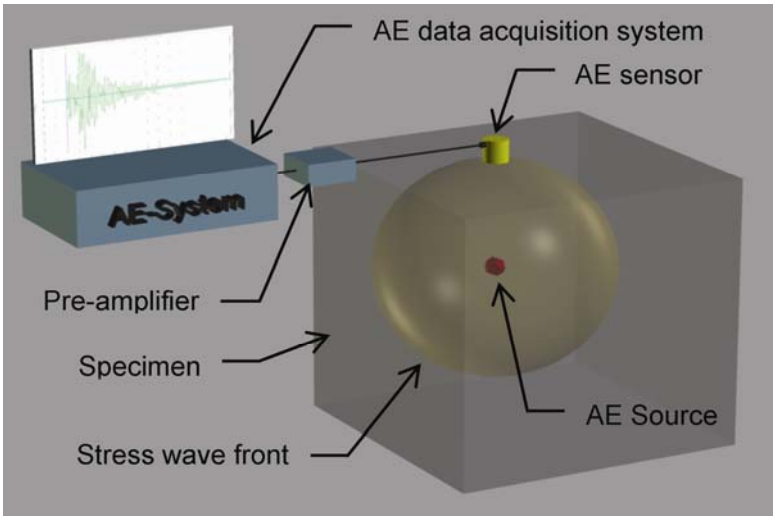

Fig. 2.1–Example of a typical AE system setup (only one AE sensor shown for clarity)

2.3 Field Experiment

2.3.1 Test Site and Procedure

The data used in this paper were collected from an in-service bridge under ambient traffic and controlled loads. The bridge is Bridge No. 7863 on Interstate 5 in Cottage Grove, OR and the tests were conducted on March 26/27, 2006. A series of ten test runs with a 22.7 t (50,000 lb) total weight three-axle dump truck were conducted with three different speeds and the response of varies sensors recorded. The bridge was closed for other traffic each time. In between the test runs, the data acquisition system was recording as well, collecting data from ambient traffic.

Fig. 2.2–Photo of the tested bridge

Fig. 2.2 shows a photo taken from the north-west corner of the bridge. The bridge is a conventionally reinforced deck girder type bridge commonly found in Oregon and was built in the 1950s. It consists of three spans plus a short cantilever span on the south side. The center span length is 25.30 m (83 ft), the adjacent spans are 19.81 m (65 ft) long, and the cantilever span length measures 3.96 m (13 ft). The wearing surface consists of a hot-mix asphalt overlay with a thickness of approximately 76 mm (3 in.).

2.3.2 Data Acquisition System and Instrumentation

The test was conducted to determine service-level strains on reinforcing bars and diagonal crack motion, as well as Acoustic Emission (AE) activity on an interior girder on the bridge. Strain was monitored on a vertical reinforcement bar (stirrup) crossing a diagonal crack with a 3.2 mm

(0.125 in.) strain gage as well crack motion perpendicular to that same crack with a 12.7 mm (0.5 in.) linear displacement sensor. A sampling rate of 10 Hz was used. The instrumentation plan is presented schematically in Fig. 2.3. AE sensors are numbered 1 through 8.

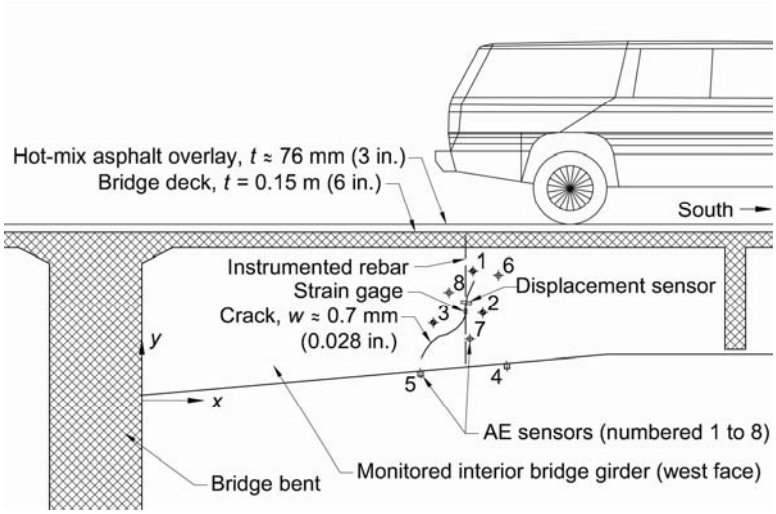

Fig. 2.3–Elevation view of monitored interior girder with sensor locations

For AE data acquisition, an eight-channel Vallen AMSY-5 system was utilized. All channels have built-in analog band-pass filters with frequency limits of 20 KHz (low) to 850 kHz (high) for channels one, seven, and eight, and 40 kHz (low) to 850 kHz (high) for channels two to six. The dynamic range of the system is 16 bit and the maximum sampling frequency 10 MHz. For this field test, wave forms were stored for all AE burst signals that crossed a threshold of 40 dB. The sampling rate was set to 2 MHz. Full AE wave forms were stored over a total length of 1024 μs with 400 μs before the threshold crossing. The AE sensors used for this test were KRNi060. They show resonant behavior with peak responses at around 60 kHz and 200 kHz. These sensors were chosen because of their high sensitivity found in laboratory experiments (Lovejoy 2006; Schumacher 2008). AE sensor location coordinates are provided in Table 2.1.

Table 2.1–AE sensor location coordinates

Sensor #	Location on face	Metric			U.S. Customary		
		x [m]	*y* [m]	*z* [m]	*x* [in.]	*y* [in.]	*z* [in.]
1	west	3.274	1.295	0.211	128.9	51.0	8.3
2	west	3.371	0.876	0.208	132.7	34.5	8.2
3	west	2.883	0.775	0.221	113.5	30.5	8.7
4	bottom	3.607	0.368	0.076	142.0	14.5	3.0
5	bottom	2.753	0.284	-0.104	108.4	11.2	-4.1
6	east	3.526	1.252	-0.206	138.8	49.3	-8.1
7	east	3.244	0.610	-0.213	127.7	24.0	-8.4
8	east	3.035	1.080	-0.218	119.5	42.5	-8.6

2.4 Data Analysis Methods

An AE system using low-frequency sensors is desirable because wearing surface and concrete have large damping characteristics. It is assumed that each individual stud impact causes a stress wave to initiate and propagate through the structure. This occurs at a frequency of about 1.3 kHz or every 0.77 ms considering a mid-sized car traveling with a speed of about 90 km/h (55 miles/h) which is in the audible range of the human ear. During the load test, audible sounds were produced by vehicles with studded tires operating on the bare surface of the bridge deck that were easily identified and distinguished by the research team. This audible signature is well known to experienced bridge and transportation engineers in regions where studded tires are used. Coincident with identification of the audible signature of the studded tires, the AE responses from this source were observed to be unique and different from other sources of AE. Subsequently, several studded-tire vehicle occurrences were identified and correlated to coincident AE patterns for further analysis.

The present AE sensor array employing eight transducers was more extensive than is actually required to identify vehicles with studded tires but commonly used for structural health monitoring. To investigate the feasibility of an automated one-channel detection system, only one sensor was considered (channel eight). Channel eight was located on the web, approximately 0.45 m (17.5 in.) below the deck. It is equipped with an analog band-pass filter that rejects frequencies below 20 kHz and above 850 kHz. Comparing the different channels, those with lower cut-off frequencies (20 kHz rather than 40 kHz) like channel eight, seemed to pick up AE from studded tires much better underlying the importance of having low frequency AE sensors.

Fig. 2.4 shows an example of recorded data from the passing of a 22.7 t (50,000 lb) three-axle test truck (a), for a passenger car equipped with studded tires (b_1) and a similar passenger car without studded tires (b_2). The top row graphs illustrate measured rebar strains (green line) and AE hit amplitudes as purple dots. The bottom row graphs show the number of detected AE hits, where the red bars represent AE hits and the green line cumulative AE hits. The bin size was set to 0.2 s. The truck's speed was about 85 km/h (52 miles/h), the cars' speeds were assumed to be in the same range. As can easily be seen in Fig. 2.4, the test truck (a) produces a large strain response with relatively low-amplitude AE hits over a time frame of approximately 2 s. On the other hand, the passenger car with studded tires (b_1) causes a small strain response accompanied by a cluster

of very high-amplitude AE with virtually no low-amplitude events over a very short time frame. The passenger car with regular tires produced a small strain response without any AE.

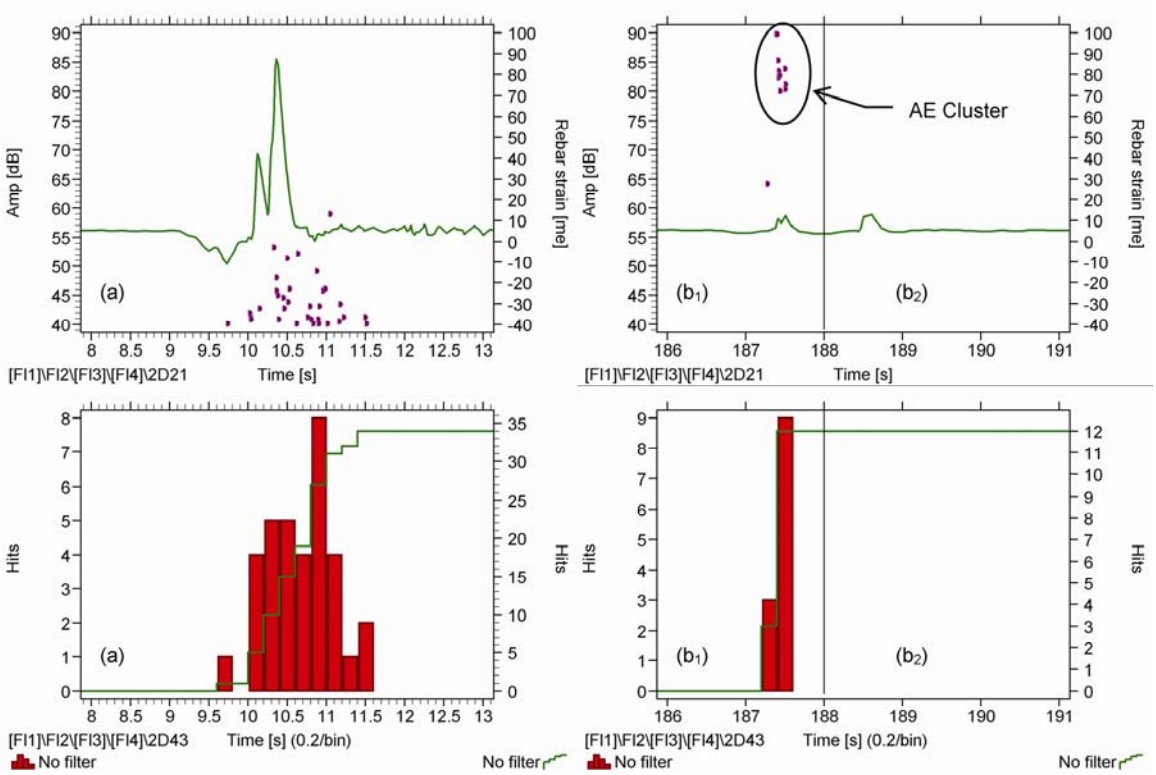

Fig. 2.4–Example data: test truck (a) and passenger car with (b_1), and without studded tires (b_2)

To summarize, vehicles equipped with studded tires were found to produce a unique response on the AE sensing system with the following characteristics:

1. Localized clusters of high-amplitude AE hits (some signals clipped due to saturation)
2. AE events occur within a very short time window
3. Small rebar strain readings

Due to the use of resonant AE sensors, there was no significant difference in the frequency response between AE signals caused from vehicles with and without studded tires. The response of such sensors is usually governed by the characteristics of the sensor and not the source.

In the following three sections, methods for data analysis are presented. Two different schemes to detect vehicles with studded tires according to the previously stated characteristics are presented and then compared.

2.4.1 Computation of AE Hit Amplitudes

AE hit amplitudes are defined as $A[dB] = 20 \cdot \log(A[mV]) + 60$, where $A[mV]$ is the maximum voltage reading from one discriminated AE burst signal. An example of a typical AE wave form is illustrated in Fig. 2.5. This output voltage is produced by the sensor's piezo-ceramic element and proportional to the surface particle motion. One issue that may arise is that the AE signals can become clipped due to channel saturation for the studded tire case. Clipped wave forms may lead to some skewing of the data for the case of the vehicles with studded tires where saturation is achieved. In this study, this was not further considered because the methods appear to be robust enough as proposed.

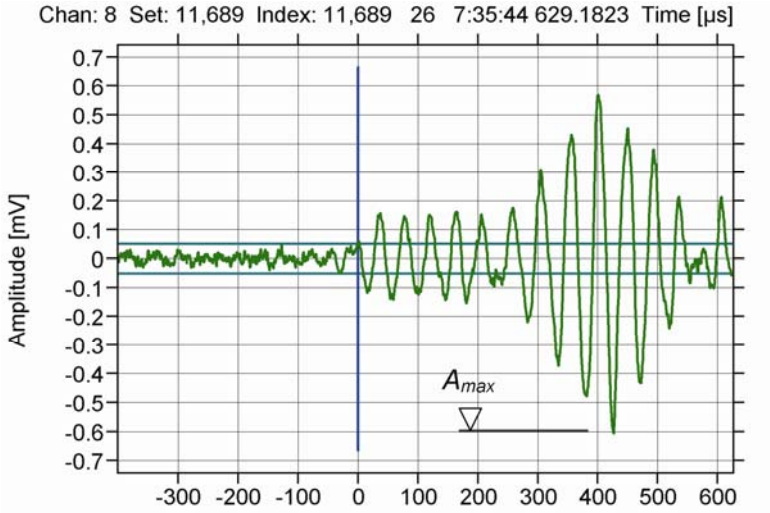

Fig. 2.5–Typical AE signal waveform

2.4.2 Detection Scheme 1: Mean AE hit amplitudes

For this scheme, mean AE hit amplitude values are computed for each discrete vehicle crossing. In addition to mean amplitude values μ, standard deviations σ were computed as well. A significant difference was found between a truck and a passenger car with studded tires in terms of average the AE hit amplitude. Fig. 2.6 shows the statistics for the AE hit amplitudes for a truck (a) and a passenger car with studded tires (b_1) computed for the same data set presented in Fig. 2.4 where *n* represents the number of AE hits included in the computation. Because there are no low-amplitude events for case (b_1), the mean value is very high and the coefficient of variation ρ

expected to be small. The coefficient of variation is defined as $CV = \sigma/\mu$. Even if the maximum AE hit amplitudes are the same for both cases, the mean for case (a) will always be lower and the spread much larger than for case (b_1) because it contains low-amplitude events. Therefore, this simple computation should be robust and work very well to detect vehicles with studded tires. However, a more complex, complementary analysis procedure for this data set is presented in the following section.

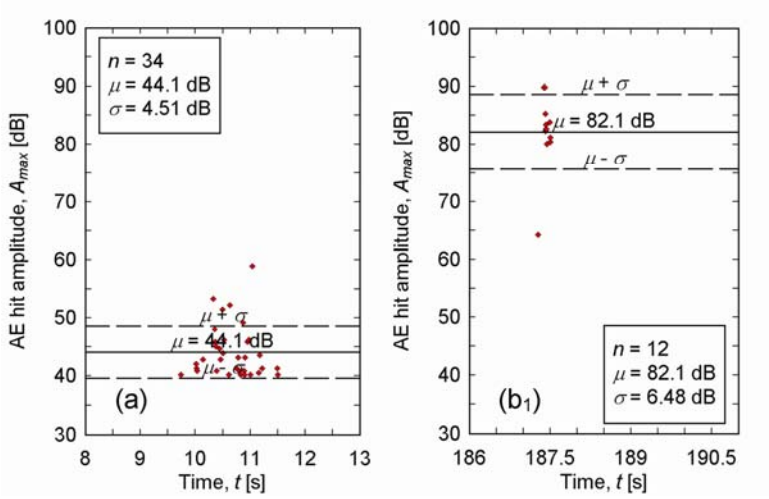

Fig. 2.6–Mean AE hit amplitudes for the test truck (a) and the car with studded tires (b_1)

2.4.3 Detection Scheme 2: *b*-Value Analysis

The observations from Fig. 2.6 indicate that the so-called *b-value analysis* or *amplitude-frequency distribution analysis* may provide an additional means to characterize vehicles with studded tires. The original relationship was established by Gutenberg and Richter (1949) to relate the annual number (mean frequency) of earthquakes with corresponding earthquake magnitudes. More recently it has been adapted to analyze slope-stability in geotechnical and material science applications (Rao and Prasanna Lakshmi 2005; Shiotani and Ohtsu 1998).

The magnitude-frequency distribution relationship is defined as:

$$\log_{10}(N) = a - bM_L \tag{2.1}$$

where M_L is the magnitude of an event on the Richter scale, N is the number of events that lie within $M_L \pm \Delta M_L$, and a and b are empirical constants. The constant b represents the slope of the magnitude-frequency diagram. The basic concept is that this b-value (the slope) decreases when damage becomes more localized. For reinforced concrete, b-value analysis has been used by several researchers to characterize structural deterioration of reinforced concrete (Colombo et al. 2003; Kurz et al. 2006; Schumacher 2008; Shiotani and Ohtsu 2000). From these studies, it was found that the b-value drops well below a value of about 1 when the system becomes unstable, i.e. during formation of a macro-crack. In AE, commonly the maximum hit amplitude in [dB] is multiplied by a factor of 1/20 and replaces the earthquake magnitude M_L. This yields b-values in the same range as those seen in seismic applications. It appears that this b-value could be used to discriminate AE event clusters caused by passenger cars with studded tires since the amplitude distribution is very distinct and different from AE clusters created by vehicles without studded tires, hence the slope or b-value should be different as well.

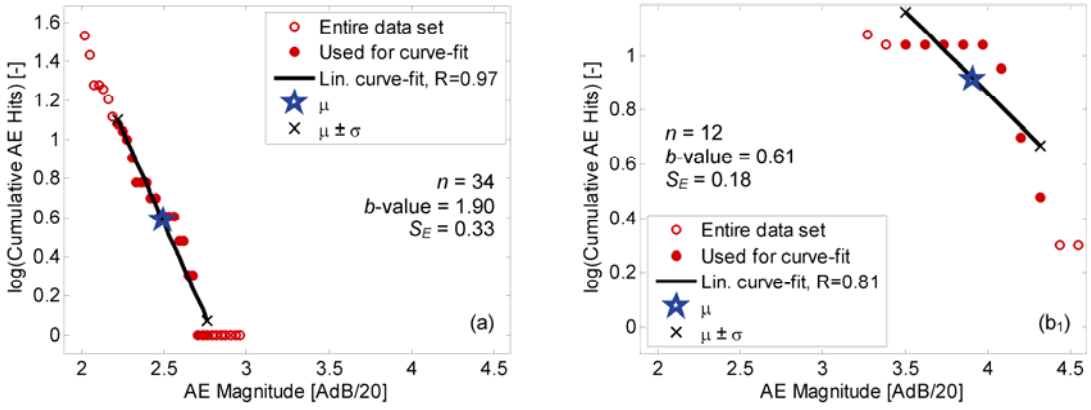

Fig. 2.7–Amplitude-frequency distributions for test truck (a) and passenger car with studded tires (b_1)

Fig. 2.7 illustrates AE amplitude-frequency distribution plots for the test truck (a) and the vehicle with studded tires (b_1). The estimated b-values of each amplitude-frequency distribution plot were estimated with Matlab employing a first order polynomial curve fit over the mean ± one standard

deviation of the AE amplitudes as suggested by Rao and Prasanna Lakshmi (2005). Standard errors are given as $S_E = b/\sqrt{n}$ where n is the number of samples used to estimate the b-values. Notice the significant difference between estimated b-values of the test truck (a) and the vehicle with studded tires (b_1). It can also be observed that the distribution line is highly non-linear for the vehicle with studded tires (b_1). This will be explored more deeply in the future as it may be used as an additional indicator to detect studded tires.

In Table 2.2, key results from the previous analyses are summarized. The differences in the sensor responses are easily recognizable. Both detection schemes, mean AE amplitudes as well as b-value analysis appear to be appropriate means to characterize vehicles with studded tires. Complementary, strain measurements can further confirm the weight magnitude and type of vehicle that is passing by the detection system.

Table 2.2–Summary of results

Parameter	(a)	(b_1)	(b_2)
Max. AE amplitude, A_{max} [dB]	59.0	89.8	0
Average AE amplitude per event, μ [dB]	44.1	82.1	0
Total hits during event, n [-]	34	12	0
Approx. time frame [s]	2	0.2	-
Estimated b-value, b [-]	1.90	0.61	-
Standard error of estimated b-value, S_E [-]	0.33	0.17	
Maximum strain, ε_{max} [με]	82	7	8
Minimum strain, ε_{min} [με]	-16	-1	-2

Analyzing clusters of AE events produced by isolated vehicle crossing is one possible way to identify vehicles with studded tires. The only problem here is that these events have to be discriminated and that can be difficult especially with dense traffic. Another alternative method is continuous evaluation of real-time AE data. The implementation of this approach is presented in the next chapter.

2.4.4 Continuous Evaluation or Real-Time Monitoring

The two previously presented analysis procedures were then implemented in Matlab and applied to the entire in-service test data. Mean AE hit amplitudes and standard deviations were computed over five values back in time. For the critical threshold, an AE amplitude value of 75 dB was

found to work well for detection of vehicles with studded tires. *b*-values were estimated over a total of 50 AE hit amplitude values back in time. A threshold was set to a critical *b*-value of 0.5 as trigger criteria for the detection of vehicles with studded tires. Once this critical *b*-value is crossed, it has to increase first above that same value before it is ready to trigger again. Verification with strain readings is then performed and has to be within a certain range that is characteristic for passenger cars with studded tires. For this study, the maximum strain reading had to be between 1 and 20 με. Because every structure is unique and has different material properties, threshold values will have to be selected on a case by case basis.

Results from the continuous evaluation are illustrated in Fig. 2.8 where (a) shows AE hit amplitudes recorded by the AE data acquisition system, (b) computed mean AE hit amplitudes (scheme 1), and (c) estimated *b*-values (scheme 2). Strain measured on the stirrup is illustrated in (d). Note that strain data is missing between approximately 6200 and 7100 s due to a small technical issue. Table 2.2 summarizes the detection results and compares them with the ones determined by manually searching through the AE hit amplitudes and strain readings for vehicles with studded tires.

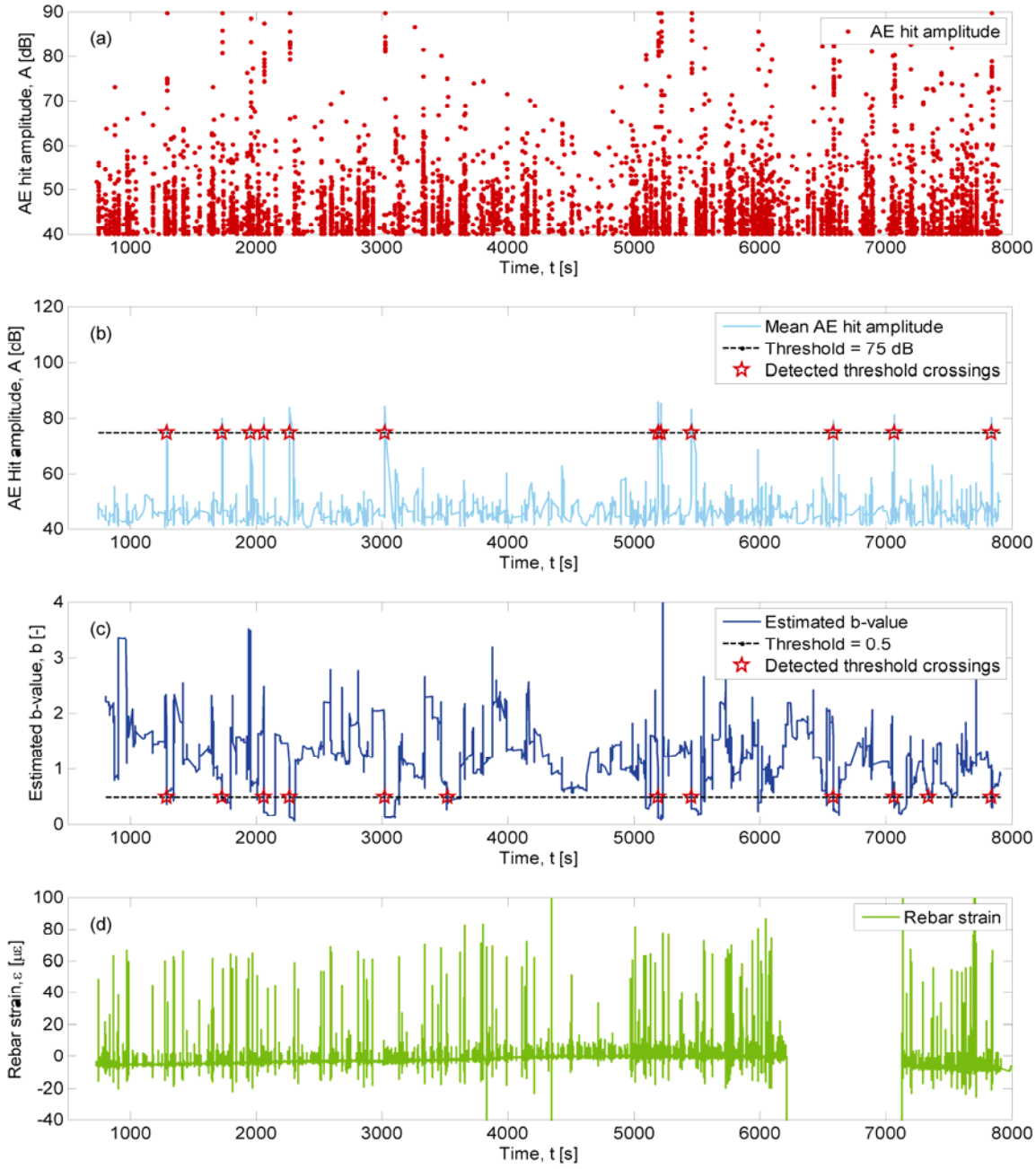

Fig. 2.8–Results for continuous evaluation

As can be seen in Table 2.3, 12 events were found manually to qualify as ‘passing vehicle with studded tires’. Detection scheme 1 (mean AE amplitudes) did an excellent job in identifying all manually determined events. Problems arise for detection scheme 2, based on *b*-values when detections have to take place closely spaced in time. This is because *b*-values need some ‘recover time’ after triggering, i.e. they have to return to a higher value of 0.5 first, before it is ready to trigger again. This problem does not exist for the mean AE hit amplitude approach (scheme 1) since the averaging is only over five AE hit amplitudes. Also, for two instances, the *b*-value scheme falsely detected vehicles with studded tires. However, the method may still be used as a complementary tool, although more fine-tuning is needed. The fact that *b*-values are sensitive to vehicles with studded tires is important by itself because this could interfere with a structural health monitoring system that monitors the structural integrity of a bridge.

Table 2.3–Summary and comparison of detection methods

Event # [-]	Manually Time [s]	Min. strain ε_{min} [με]	Max. strain ε_{max} [με]	Scheme 1 Time [s]	Scheme 2 Time [s]
1	1290	-1	7	1291	1290
2	1726	-1	7	1726	1726
3	1955	-1	8	1955	-
4	2059	-2	11	2059	2059
5	2264	-2	9	2264	2264
6	3023	-1	5	3023	3023
7	-	-2	6	-	3524
8	5190	-1	7	5190	5190
9	5217	-1	10	5216	-
10	5457	-1	10	5457	5457
11	6579	n/a	n/a	6579	6579
12	7069	n/a	n/a	7069	7069
13	-	-1	8	–	7338
14	7836	-3	16	7836	7836
Detections, total	12	-	-	12	12
Correct detections	-	-	-	12	10
Not detected, missed	-	-	-	0	2
False detections	-	-	-	0	2

2.4.5 Recommendations for an Integrated Detection System

A practicable implementation of a detection system for vehicles with studded tires is described here. As shown earlier, a conventional one-channel AE detection system would be sufficiently robust to detect passing vehicles with studded tires. An AE sensor would be mounted to the deck soffit to maximize detection. This sensor would be connected via coax-cable to the single-channel AE system located in an accessible and secured enclosure. Hand-held one-channel AE systems are commercially available that would work for this kind of application. Additionally, a strain gage could be used as a supplemental parametric input for verification of the vehicle load effect. However, the authors suggest the use of a wireless sensor network employing so-called motes would be especially energy efficient and low maintenance for this application. A mote is a complete measurement and communication unit that connects to the sensor via a short cable and communicates with a base station via radio transmission (Grosse et al. 2006). The base station would be located at the site and be triggered by pre-defined threshold values of the mean AE hit amplitudes. From here, the data would be either stored locally at the site to be manually collected or streamed to a central server (via cable, radio transmission, or cell phone) for continuous observation or analysis. Alternatively, messages could be sent regularly to the bridge owner as to cumulative counts and times of occurrences. Further, a camera positioned over the roadway could be triggered to capture images of the identified vehicles for reference. At the present time, the technologies exist and are practically obtained for such systems and at reasonable cost.

2.5 Conclusions

The use of studded tires has become of increasing concern to transportation agencies due to the damage caused to pavements, and limited funds available for repair and replacement. Large annual expenditures are made in jurisdictions which permit studded tires to maintain pavements. Currently no tools are available to automatically detect and report vehicles with studded tires. An integrated system to detect vehicles with studded tires passing over a highway bridge is proposed. Piezo-electric sensors attached to the bridge members can detect and record stress waves that are emitted when vehicles with studded tires pass over the bridge. Discrimination of these stress waves is possible because they were found to significantly differ from trucks and vehicles that have no studded tires. It was found that simple mean AE hit amplitude schemes work very well and are sufficient to detect vehicles with studded tires that pass over a bridge. Nevertheless, physical measurements as rebar or surface strain readings are recommended as complimentary measurement of load magnitude. Additional analysis methods, such as *b*-value analysis are sensitive to vehicles with studded tires as well, but need some further fine tuning.

A simplified single-channel system could be practicably deployed for detection and reporting and would allow for collection of statistical data to better estimate pavement life and wear ratio. AE systems offer the opportunity for more reliable data on the number of studded tires in operation and the time periods of use on a particular highway. That can be utilized primarily to improve design and maintenance of road surfaces. The system could further be extended for use as an enforcement tool of legal studded tire operating dates.

2.6 Acknowledgements

The support and sponsorship for this study by the Oregon Department of Transportation is greatly appreciated.

2.7 References

Angerinos, M. J., Mahoney, J. P., Moore, R. L., and O'Brien, A. J. (1999). "A Synthesis on Studded Tires." Washington State Transportation Center (TRAC), Olympia, WA.

Brunette, B. E., and Lundy, J. R. (1996). "Use and Effect of Studded Tires on Oregon Pavements." Transportation Research Record, National Academy Press, Washington, D.C., 64-72.

Colombo, S., Forde, M. C., Main, I. G., and Halliday, J. (2003). "AE monitoring of concrete bridge beams in situ." *The Structural Engineer*, 81(23), 41-46.

EN. (2000). "1330-9: Non-destructive testing-Terminology-Part 9: Terms used in acoustic emission testing." European Committee for Standardization (CEN), Brüssel, Belgium.

Grosse, C. U., Glaser, S. D., and Krüger, M. (2006). "Condition Monitoring of Concrete Structures Using Wireless Sensor Networks and MEMS." SPIE Smart Structures and Materials: Sensors and Smart Structures Technology for Civil, Mechanical, and Aerospace Systems, 407-418.

Gutenberg, B., and Richter, C. F. (1949). *Seismicity of the earth and associated phenomena*, Princeton University Press, Princeton, NJ.

Kurz, J. H., Finck, F., Grosse, C. U., and Reinhardt, H.-W. (2006). "Stress Drop and Stress Redistribution in Concrete Quantified Over Time by the b-value Analysis." *Structural Health Monitoring*, 5(1), 69-81.

Lovejoy, S. C. (2006). "Development of Acoustic Emissions Testing Procedures Applicable to Convetionally Reinforced Concrete Deck Girder Bridges Subjected to Diagonal Tension Cracking," PhD Dissertation, Oregon State University, Corvallis, OR.

Malik, M. G. (2000). "Studded Tires in Oregon-Analysis and Pavement Wear and Cost of Mitigation." Oregon Department of Transportation, Salem, OR.

Miller, R. K., Hill, E. v. K., and Moore, P. O. (2005). *Nondestructive Testing Handbook - Volume 6 - Acoustic Emission Testing*, American Society for Nondestructive Testing (ASNT), Columbus, OH.

Rao, M. V. M. S., and Prasanna Lakshmi, K. J. (2005). "Analysis of b-value and improved b-value of acoustic emissions accompanying rock fracture." *Current Science*, 89(9), 1577-1582.

Schumacher, T. (2008). "Acoustic Emission Techniques Applied to Conventionally Reinforced Concrete Bridge Girders." Oregon Department of Transportation (ODOT), Salem, OR.

Shiotani, T., and Ohtsu, M. (1998). "Prediction of Slope Failure Based on AE Activity." Acoustic Emission: Standards and Technology Update, ASTM STP 1353, American Society for Testing and Materials, 156-171.

Shiotani, T., and Ohtsu, M. (2000). "Prediction of Slope Failure Based on AE Activity." Acoustic Emission: Standards and Technology Update - ASTM STP 1353, West Conshohocken, PA, 156-171.

WSDOT. (2006). "Pavements and Studded Tire Damage." Washington Department of Transportation (WSDOT)-Materials Laboratory, Olympia, WA.

Zubeck, H., Larson, E., Aleshire, L., Harvey, S., and Porhola, S. (2004). "Socio-Economic Effects of Studded Tire Use in Alaska." State of Alaska, Anchorage, AK.

Estimating Operating Load Conditions on Reinforced Concrete Highway Bridges with *b*-Value Analysis from Acoustic Emission Monitoring

Thomas Schumacher, Christopher C. Higgins, and Steven C. Lovejoy

Structural Health Monitoring
SAGE Publications
2455 Teller Road
Thousand Oaks, CA 91320
USA

Accepted for publication on October 5, 2009

3 Second Manuscript

Estimating Operating Load Conditions on Reinforced Concrete Highway Bridges with *b*-Value Analysis from Acoustic Emission Monitoring

Thomas Schumacher[1], Christopher C. Higgins[2], and Steven C. Lovejoy[3]

Abstract: Transportation agencies commonly have conventionally steel reinforced concrete deck girder (RCDG) bridges in their inventory that were built in the mid-twentieth century. These bridges have been in-service beyond their intended design lives and tools are needed to permit freight mobility and maintain operational safety. The practical applicability of AE monitoring techniques were investigated to help estimate the condition of diagonally cracked RCDG bridges. Experiments on two full-scale girder specimens representative of Oregon's RCDG bridges were built and tested under realistic service conditions. Overloading conditions were imposed to increase the level of deterioration. It was found that characterizing the current health condition of a monitored bridge component or element based on short term in-service loading is difficult and the proximity of a potential bridge failure not easily predictable until it is impending. However, it was observed that the current operating load level of a bridge component can be estimated using a newly proposed method called *Minimum b-Value Analysis*. The influence of factors that can affect *b*-value estimations such as stage of deterioration or external sources was studied and is introduced. The experiment as well as data from the two laboratory specimens are presented and interpreted.

Keywords: Operating load conditions, In-service load testing, Reinforced concrete bridges, Acoustic Emission Monitoring, *b*-Value analysis

[1] Graduate Research Assistant, School of Civil and Construction Engineering, Oregon State University, USA; E-mail: schumact@engr.orst.edu

[2] Professor, School of Civil and Construction Engineering, Oregon State University, USA; E-mail: chris.higgins@oregonstate.edu

[3] Senior Research Engineer, Oregon Department of Transportation, Bridge Engineering Section, Salem, OR, USA; E-mail: steven.c.lovejoy@odot.state.or.us

3.1 Introduction and Background

Many transportation agencies have conventionally reinforced concrete deck girder (RCDG) bridges in their inventory that were built during the highway expansion in the 1950s. The anticipated design life was 50 years and many of them have reached their intended service-life limit. These bridges commonly exhibit diagonal tension cracking in the high shear regions of the girders that can mostly be attributed to the increasing volume of heavy truck traffic and environmental factors. Conventional load rating methods often identify many of these structures to be deficient for current loading conditions. As an example, in Oregon a very large bridge replacement program was initiated in 2003, with a total cost exceeding 1.6 billion US dollars. However, these resources are insufficient to replace all the cracked bridges and large numbers of these will be required to remain in-service (Kuennen 2006). A need exists to better predict the capacity and remaining life for RCDG bridges that will stay in service to prioritize future replacements and impose load restrictions when required. A research project was launched to evaluate and estimate the remaining life of RCDG bridges (Higgins et al. 2004a; Higgins et al. 2004b). Acoustic Emission (AE) testing was chosen as a non-destructive testing method to further assist with addressing the problem (Lovejoy 2006; Schumacher 2008).

Reinforced concrete (RC) bridges generally operate at service-level loads except during discrete overload events that can reduce the integrity of the structure by initiating concrete cracks, widening or extending existing concrete cracks, as well as producing reinforcing steel slip or yielding. Identification of previous damage and predicting the possible impact on future performance has increasingly become of interest to load rating engineers. One of the goals of the recently completed research by Schumacher (2008) was to determine if AE techniques can assist in (1) assessing and identifying previous damage, (2) monitoring existing bridges for real-time detection of damage occurrence, and (3) predicting critical conditions or failure of bridge members. The term damage in this context shall be defined as a change in the current state or condition of a structural element that reduces its capacity. Damage is not a well-defined term for reinforced concrete since cracking alone does not necessarily reduce the ultimate capacity of a member. However, crack formation and crack width growth are of importance since they may lead to bond fatigue or expose steel reinforcement to the environment which can lead to rebar corrosion, etc. that may reduce capacity. In the present study, the term deterioration is therefore used rather than damage.

3.2 Overview of Full-Scale Laboratory Experiments

3.2.1 Test Specimens

Two full-scale test beams representative of in-service bridges were fabricated and subsequently tested under realistic loading conditions as discussed subsequently in the structural laboratory. The overall length of the T-girders was 7.92 m (26 ft), the total height 1.22 m (4 ft), the flange width 914 mm (36 in.), and the web thickness 356 mm (14 in.). Illustrated in Fig. 3.1 is a cross-section at the center line of the beam specimens used in this project. They were tested in IT-configuration, imposing flexural tension in the deck to reflect the high-shear, high-negative moment region common in these structurally continuous bridges. No skin steel was added to the reinforcing cage to reflect 1950s detailing practices. The stirrups were manufactured from Grade 40 (f_y = 276 MPa), all other of Grade 60 (f_y = 414 MPa) reinforcing steel. The specimens were named AE Specimen #1 and #2. For AE Specimen #1, all 6 ø 35 mm (#11) longitudinal tension rebars were well anchored past the supports on both sides, whereas for AE Specimen #2, the two outer rebars were cut-off at 2.13 m (7 ft) from the center line of the specimen. These cut-offs were common practice to optimize the steel needed to provide for the flexural demand on the member. The ø 13 mm (#4) transverse reinforcing bars (stirrups) were uniformly spaced at 305 mm (12 in.) in the high shear region of interest.

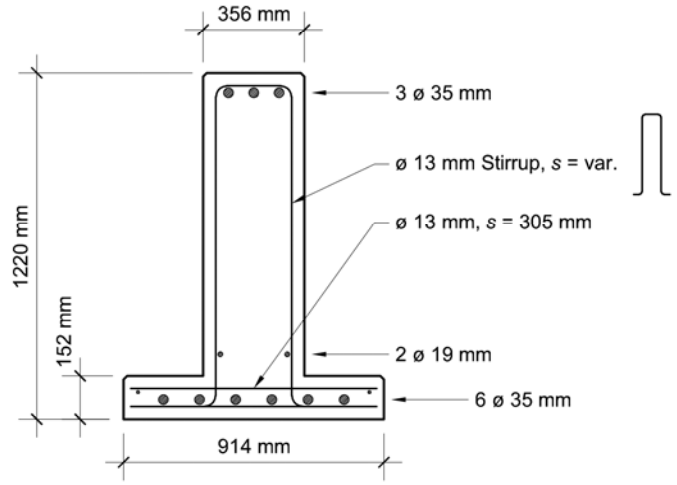

Fig. 3.1–Specimen cross-section shown in inverted T (IT) configuration

3.2.2 Experimental Setup

The tests were performed with a four-point loading configuration. Force was applied at mid-span through a spreader beam to load points on the specimen spaced 610 mm (24 in.) apart. The spacing between the supports (span length) was 6.60 m (21 ft 8 in.). Applied force was measured with a 2200 kN (500 kips) capacity load cell mounted to the hydraulic actuator. The experiments were conducted with a closed-loop servo-hydraulic system in the force-controlled mode. The setup used for all tests is illustrated in Fig. 3.2. To minimize noise from the test frame interfering with the AE measurements, neoprene strips were installed between all bearing surfaces (see inset 'Detail A').

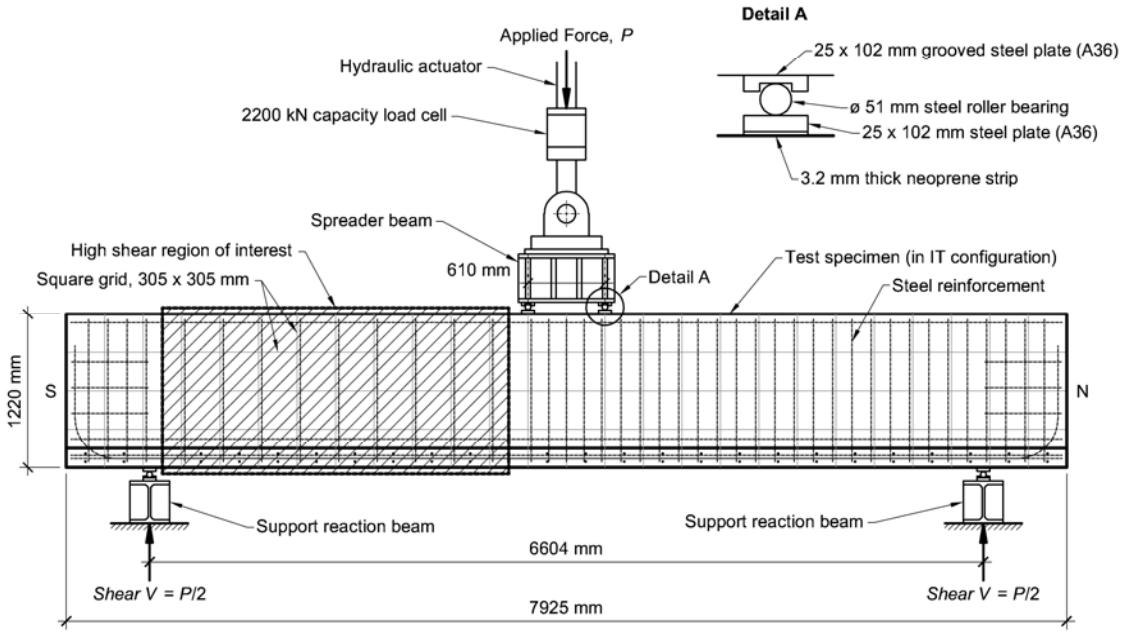

Fig. 3.2–Test setup configuration for both AE Specimens

Eight 60 kHz resonant AE sensors were deployed in two different arrays (A and B) to record stress waves generated during testing. The array used for the present study employed for AE Specimen #1 and #2 was array A and is schematically shown in Fig. 3.3. The sensors were arranged in an anti-symmetric manner around the high shear region of interest. For AE data acquisition, a commercially available eight-channel system was used. For AE Specimen #2, AE

transducers were only placed at or above the center height of the girder ($y \geq 0$). This was done so that crack interference may be prevented for as long as possible.

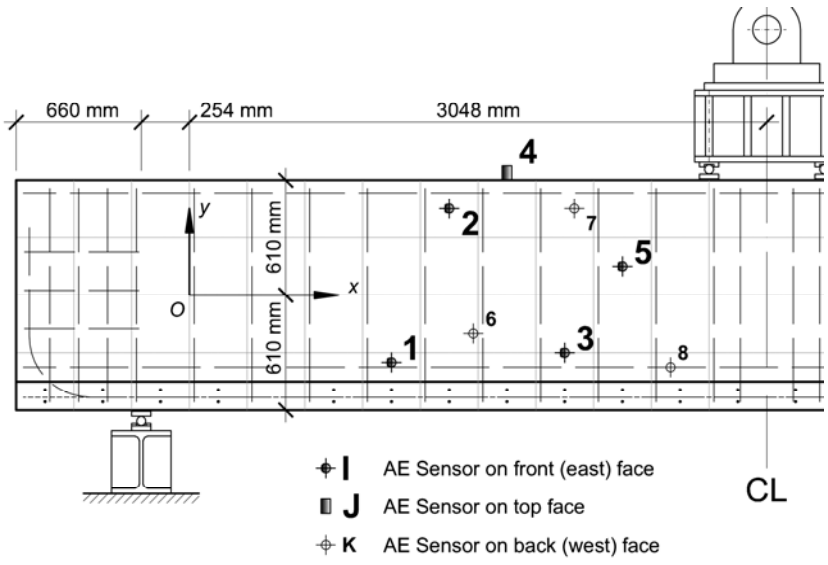

Fig. 3.3–AE sensor locations for sensor array A (schematically) for the two AE Specimens

Additionally, data from over 30 conventional sensors were collected. These included load cells, strain gages, concrete clip gages to measure crack motion (CMOD), and displacement sensors. Strain gages were bonded to selected stirrups (vertical shear reinforcement) at mid-height in the high shear region of interest (as highlighted in Fig. 3.2) and installed prior to casting of concrete. Flexural reinforcing bars were instrumented with strain gages at mid-span and at rebar cut-off locations.

3.2.3 Loading Protocol

Most of the AE research in laboratories has used loading protocols of loading and unloading cycles with each subsequent increment applied at higher load magnitude, e.g. (Colombo et al. 2003). Repeated cyclic loading at service level or fatigue loading have rarely been considered. However, such loading history may change the AE response significantly as it helps redistribute residual stresses after an overload event, for example. One goal of this research was to develop and employ a loading protocol that is representative of realistic service-level load conditions and

can therefore be directly compared with in-service load tests. In that sense, the present work should serve as a reference for future field work.

Another distinguishing feature that was considered was the unloading effect (live load strain reversal) that was found in the rebar strain readings during typical in-service load tests before the main maximum strain reading (tensile) occurred. This was observed for instrumented stirrups close to supports (high shear region) when the truck approached that section just before crossing it. In addition, the cracks close when the load was located directly above the section. This stirrup unloading effect was taken into account and applied to the lab specimens using a rounded value of 20% of the subsequently applied peak load.

The applied force for the simulated test trucks was based on the structural analysis of a typical continuous 15 m (50 ft) 3-span continuous bridge. Distribution factors were taken from Potisuk and Higgins (2007). The shear force effect due to dead load was estimated at 178 kN (40 kips) which corresponds to a total applied force of 356 kN (80 kips). Fig. 3.4 illustrates the first load phase and the beginning of the second load phase that were applied to both, AE Specimen #1 and #2. Notice the small unloading portion discussed previously that appears before every load cycle.

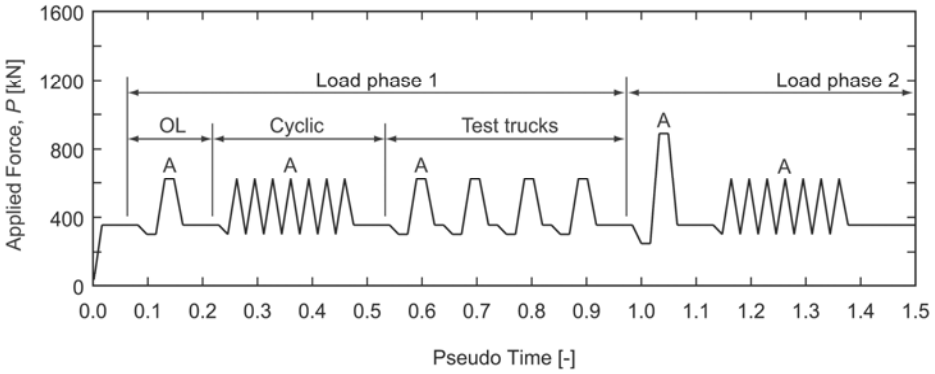

Fig. 3.4–Generalized loading protocol (‘A’ stands for ‘sensor array A’ as presented in Fig. 3.3)

The following general loading procedure was applied to both specimens as illustrated in Fig. 3.4:

1. Apply equivalent dead load (DL) to specimen representative of service-level conditions.
2. Impose new deterioration by applying a monotonic overload (OL) force followed by unloading to DL.
3. Apply load cycles at service-level to reach steady-state strain response.
4. Load specimen with simulated test trucks (TT) to replicate in-service load-testing of actual bridges.
5. Go back to step 2, applying a higher load level to impose new deterioration into the specimen.

The simulated test trucks ranged from total applied forces of 623 to 1068 kN (140 to 240 kips) which corresponds to shear effects on the section of 312 to 534 kN (70 to 120 kips). The simulated test truck magnitude (623 kN (140 kips)) was selected based on produced load effects on the section that are within the range of those available to almost all transportation agencies. Higher ones were introduced in later load phases in increments of 89 kN (20 kips) because the basic TT caused less and less AE activity with increasing deterioration (at higher overload phases). Commonly, loaded maintenance trucks are used for structural in-service load tests with total weights of approximately 18 to 25 tons. This procedure was continued until the specimens were failed. The capacity and failure mode of AE Specimen #1 could not be determined experimentally since the spreader beam slipped off the specimen when reaching an applied force of 1605 kN (361 kips) corresponding to a shear force of 803 kN (180 kips). The capacity (ultimate shear force) was estimated to be approximately 1780 kN (400 kips) using Response 2000 which has been shown to provide excellent prediction for these specimens (Higgins et al. 2004a). The capacity of AE Specimen #2 was found experimentally at a total applied force of 1658 kN (373 kips) which corresponds to a shear capacity of 829 kN (186 kips). Failure occurred in shear-compression mode. Response 2000's predicted strength for AE Specimen #2 was 1664 kN (374 kips) and corresponds very well with the experimental value. The different load phases of the experiment with maximum applied overloads (OL), corresponding shear, and applied simulated service-level test trucks (TT) on the section are summarized for both test specimens in Table 3.1.

The following load ratios are used subsequently in this paper to normalize forces:

$$LR1 = \frac{Applied\ \ force}{Ultimate\ capacity} \tag{3.1}$$

$$LR2 = \frac{Applied\ \ force}{Previous\ applied\ overload} \tag{3.2}$$

$$LR3 = \frac{Previous\ applied\ overload}{Ultimate\ capacity} \tag{3.3}$$

Table 3.1–Summary of applied OLs and TTs for both specimens
(AE Specimen #1 and #2)

Load phase [-]	Force *OL* [kN]	Shear V_{corr} [kN]	AE #1 *LR3* [-]	AE #2 *LR3* [-]	*Number of same magnitude TTs AE #1/AE #2* 623 [kN]	712 [kN]	801 [kN]	890 [kN]	979 [kN]
1	623	312	0.35	0.38	3/3	-/-	-/-	-/-	-/-
2	890	445	0.50	0.54	3/3	-/3	-/3	-/-	-/-
3	1156	578	0.65	0.70	3/5	3/3	3/3	-/3	-/3
4 (#1)	1423	712	0.80	-	4/-	3/-	3/-	3/-	3/-
4 (#2)	1468	734	-	0.88	-/3	-/3	-/3	-/-	-/3
5 (#1)	1605	803	0.90[1]	-	-/-	-/-	-/-	-/-	-/-
5 (#2)	1658	829	-	1.00[3]	-/-	-/-	-/-	-/-	-/-
5 (#1)	1780	890	1.00[2]	-	-/-	-/-	-/-	-/-	-/-

[1] Spreader beam slips off specimen, termination of test
[2] Ultimate capacity estimated using Response 2000 (never reached)
[3] Ultimate capacity (experimentally determined)

3.2.4 Specimen Response

Figs. 3.5 and 3.6 show cracks that were mapped at the beginning of each load phase. Generally, vertically oriented flexural cracks formed at a total applied force of approximately 320 kN (72 kips), i.e. below the total applied force due to dead load of 356 kN (80 kips). While imposing the first overload cycle, the first inclined shear cracks formed. This occurred at an applied force of approximately 420 kN (94 kips) for both specimens. After that, with every new overload, existing cracks propagated further towards the compression zone and branched. One difference in the crack formation between the two specimens was that during load phase 3 for AE Specimen #2, a completely new crack (marked with an arrow in Fig. 3.6, bottom left) formed in a previously

uncracked region in the middle of the high shear region. Interestingly, this later forming crack was not part of the eventual failure crack.

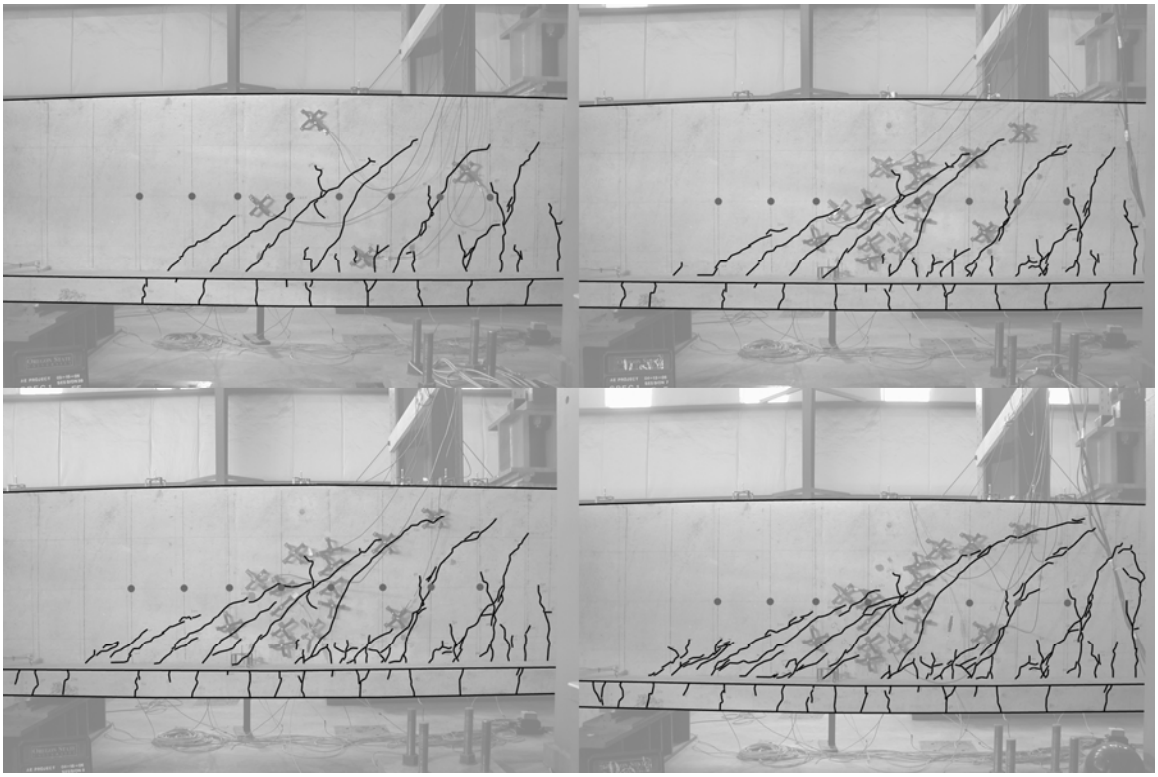

Fig. 3.5–Mapped cracks at the beginning of each load phase for AE Specimen #1
Top left: load phase 1, *LR3* = 0.35
Top right: load phase 2, *LR3* = 0.50
Bottom left: load phase 3, *LR3* = 0.65
Bottom right: load phase 4, *LR3* = 0.80

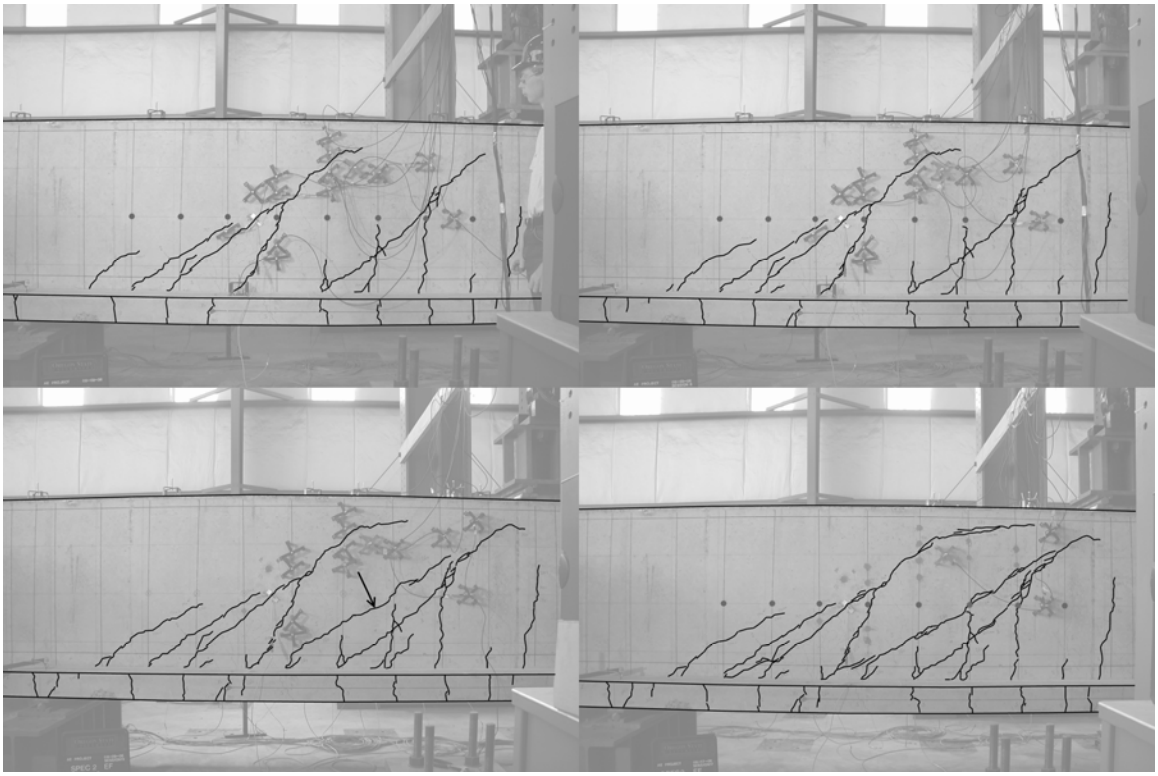

Fig. 3.6–Mapped cracks at the beginning of each load phase for AE Specimen #2
Top left: load phase 1, *LR3* = 0.38
Top right: load phase 2, *LR3* = 0.54
Bottom left: load phase 3, *LR3* = 0.70
Bottom right: load phase 4, *LR3* = 0.88

In Fig. 3.7, load phase 2 for AE Specimen #2 is shown as a typical example for the measure AE response. It can be observed that the AE hit rate is very large, i.e. approximately 1100 AE hits per second for the applied overload (left Fig.). The subsequent cyclic loading employed to simulate ambient traffic (in this case 2 x 1000 cycles) shows a relatively steady AE hit rate. The following simulated test trucks (right Fig.) produced much lower AE hit rates due to the low demand on the section relative to the initial overload. It shall also be pointed out that the AE hit rate is actually decreasing for subsequent TTs of the same magnitude, e.g. for the 801 kN (180 kips) TT in the right Fig.. This is due to the uniqueness of AE events.

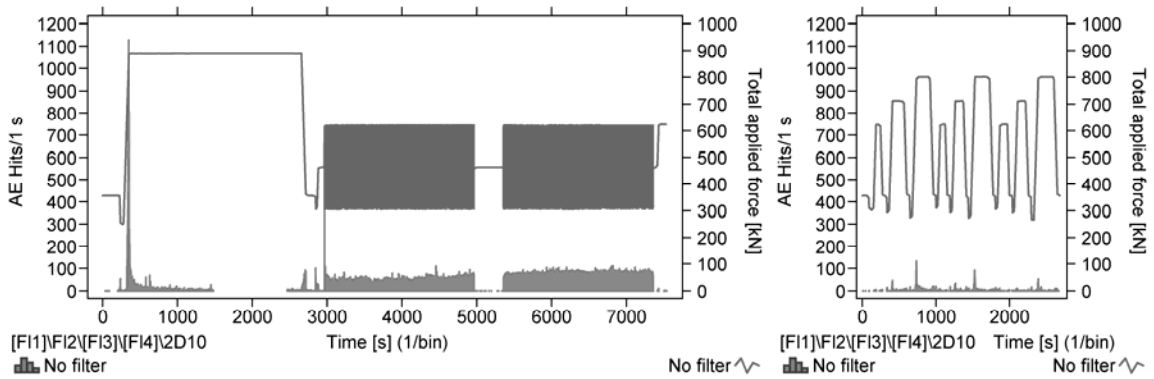

Fig. 3.7–Example of applied OL and subsequent cycles (left Fig.) and TT (right Fig.), both also showing AE hit rates (forces are applied total forces)

The ranges of physical measurements such as rebar strains, diagonal displacements, and crack motions remained fairly constant (difference < 2%) over a series of equally heavy applied simulated test trucks. Maximum stirrup strains ranged between approximately 300 and 900 με (which corresponds to a stress range of approximately 60 to 180 MPa (8.7 to 26 psi), depending on the applied force and the stage of deterioration (or phase). The *b*-value response on the other hand varied up to 25% for some test truck groups. It is therefore very important to provide experimental results that can show some measure for data uncertainty (e.g. variance) and not just the mean result or prediction line alone.

3.3 Acoustic Emission Testing Using Minimum *b*-Values

3.3.1 Background and Introduction

The general principle of AE testing is that emitted stress waves caused by sudden internal strain release processes due to loading of the structure are recorded, stored, and then analyzed (Grosse and Ohtsu 2008; Miller et al. 2005). Piezo-electric sensors mounted to the surface convert transient surface displacements produced by arriving stress waves into an electrical signal. Usually not only one but several sensors are deployed as an array and data are recorded in parallel. Typically, pre-selected minimum amplitude threshold values are used to trigger the system for individual AE burst signals from which descriptive AE parameters such as maximum signal amplitude, energy of the signal, signal duration, or rise time (time between threshold crossing and maximum signal amplitude) are extracted for qualitative analyses. For quantitative analysis procedures, full AE signal wave forms are recorded and stored with sampling frequencies up to 10 MHz. All this is done in real-time and requires a powerful data acquisition system. The most important point to keep in mind is that stored AE data are influenced by many factors in the measurement process chain, e.g. sensor and material characteristics, cracks and crack development over time, and the data acquisition settings. It was thus very important for this project to establish crucial boundary conditions (sensor array geometry, selection of sensors) and data acquisition settings (AE amplitude threshold values) that are consistent for both the laboratory experiment and that which could be used for in-service field tests of bridge girders in order to provide linkages between results.

For the present study, a commercially available eight channel Vallen AMSY-5 AE data acquisition system was employed. All eight channels were equipped with analog band-pass frequency filters that reject frequencies below 20/40 kHz and above 850 kHz. The piezo-electric AE transducers used for all experiments were 60 kHz resonant type (model KRNi060), manufactured by KRN Services. These have shown good sensitivity for applications in RC (Lovejoy 2006; Schumacher 2008). Amplitude threshold values during data acquisition were selected depending on the expected background noise level and AE intensity. For final data analysis, a post-processing high-pass filter was set to a fixed value of 40 and 44 dB to achieve consistency across the different experimental phases for AE Specimen #1 and #2, respectively. AE signal wave forms were recorded with a sampling frequency of 2.0 MHz and stored for reference.

3.3.2 Introduction to *b*-Value Analysis

A statistical method used to look at parametric AE data is the so-called *b*-value analysis. The relationship was first established by Gutenberg and Richter (1949) and has been used to characterize distributions of earthquake magnitudes (Stein and Wysession 2003) as well as to analyze slope-stability in geotechnical (Miller et al. 2005; Rao and Prasanna Lakshmi 2005; Shiotani and Ohtsu 1998) and material science applications for a variety of materials (Carpinteri et al. 2009; Cox and Meredith 1993; Hardy 1971; Kurz et al. 2006; Pollock 1981; Shiotani et al. 2000). The empirical magnitude-frequency distribution relationship is defined in logarithmic form as:

$$\log_{10}(N) = a - bM_L \tag{3.4}$$

where M_L is the magnitude of an event on the Richter scale, N is the number of events that lie within $M_L \pm \Delta M_L$, and a and b are empirical constants, where b describes the slope of a fitted straight line of the magnitude-frequency diagram or ratio of small and large earthquake magnitudes (Stein and Wysession 2003). The basic concept relies on the change of the *b*-value (the slope) to indicate changes in the indulging material. The *b*-value shows these changes as a decrease in slope below a value of approximately 1.0 when stresses are redistributed and damage becomes more localized. In the field of reinforced concrete, *b*-value analysis has been studied by several researchers to monitor structural deterioration using AE monitoring (Colombo et al. 2003; Kurz et al. 2006; Miller et al. 2005; Shiotani et al. 2000). Commonly in AE applications, the maximum hit amplitude in dB is multiplied by a factor of 1/20 and replaces the earthquake magnitude M_L (Colombo et al. 2003; Weiss 1997). This yields *b*-values in the same range as seen in seismic applications. The *b*-value for each set of AE amplitude-frequency distributions was estimated employing a linear least squares curve-fit over the mean ± one standard deviation as employed by Colombo et al. (2003) and also suggested by Rao and Prasanna Lakshmi (2005). Standard errors, S_E are given as $b/\sqrt{n}$ where n is the number of samples used (consecutive AE hit amplitudes used for the estimation). Suggested values for n found in the literature range from 50 to 100 (Colombo et al. 2003; Kurz et al. 2006; Rao and Prasanna Lakshmi 2005). Fig. 3.8 visualizes what *b*-values represent: the slope of the cumulative amplitude-frequency distribution of a set of AE hit amplitudes. The *b*-value changes when the ratio of the number of strong to

weak AE events changes. High and low *b*-values have been associated with micro-crack formation (distributed deterioration) and macro-crack formation and propagation (localized deterioration), respectively, as proposed in (Carpinteri et al. 2006; Cox and Meredith 1993; Kurz et al. 2006; Pollock 1981; Rao and Prasanna Lakshmi 2005; Rundle et al. 2003). For this example, two sets of 50 consecutive AE hit amplitudes at different instances were selected from AE Specimen #2 during load phase 2.

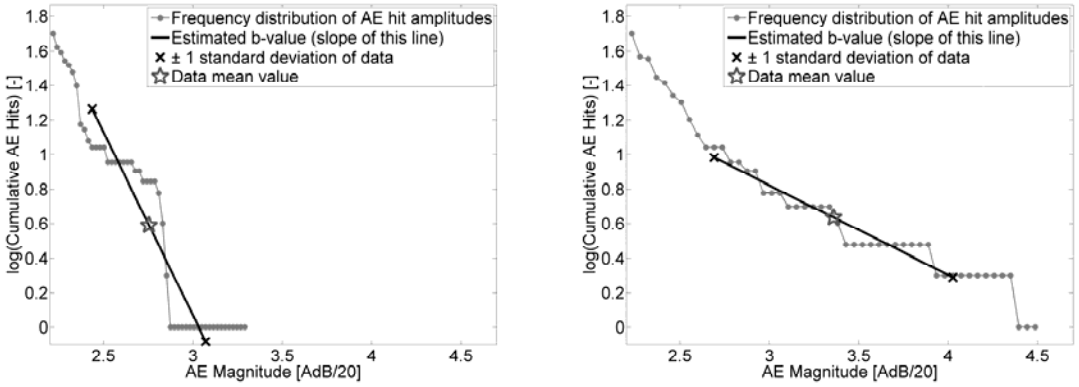

Fig. 3.8–Examples of two estimated *b*-values with 50 consecutive AE hit amplitudes:
Left Fig.: likely no on-going deterioration or micro-cracking (*b*-value = 2.12, S_E = 0.30)
Right Fig.: likely on-going deterioration or macro-cracking (*b*-value = 0.52, S_E = 0.07)

Two main sources of AE in concrete are present that are of interest. When the material is loaded for the first time, micro-cracks form in highly stressed regions. They are distributed, small and generate a large number of low amplitude AE events which should produce a *b*-value well above 1.0. Once concrete reaches its tension cracking stress, a localized macro-crack is initiated that produces a relatively small number of high amplitude AE events which should produce a *b*-value well below 1.0. These two types of AE sources cause AE with different amplitudes and frequency distributions. Also, in reinforced concrete, the reinforcing steel is designated to carry the released tension concrete stress once a macro-crack forms. Once that has occurred, a third source of AE may be present due to the relative crack motion of the two crack surfaces during repeated in-service loading. This is possible when loosened cementitious material parts from the crack surface or even entire aggregates get in between the crack surfaces and are crushed or cause crushing of neighboring material. This third source can occur at any point during the life-time of a structure and may be accelerated by environmental effects further increasing the number of low

amplitude AE events. For service-level load effects, these are most likely the main sources of AE since the material is usually not stressed enough to produce either micro- or macro-cracks.

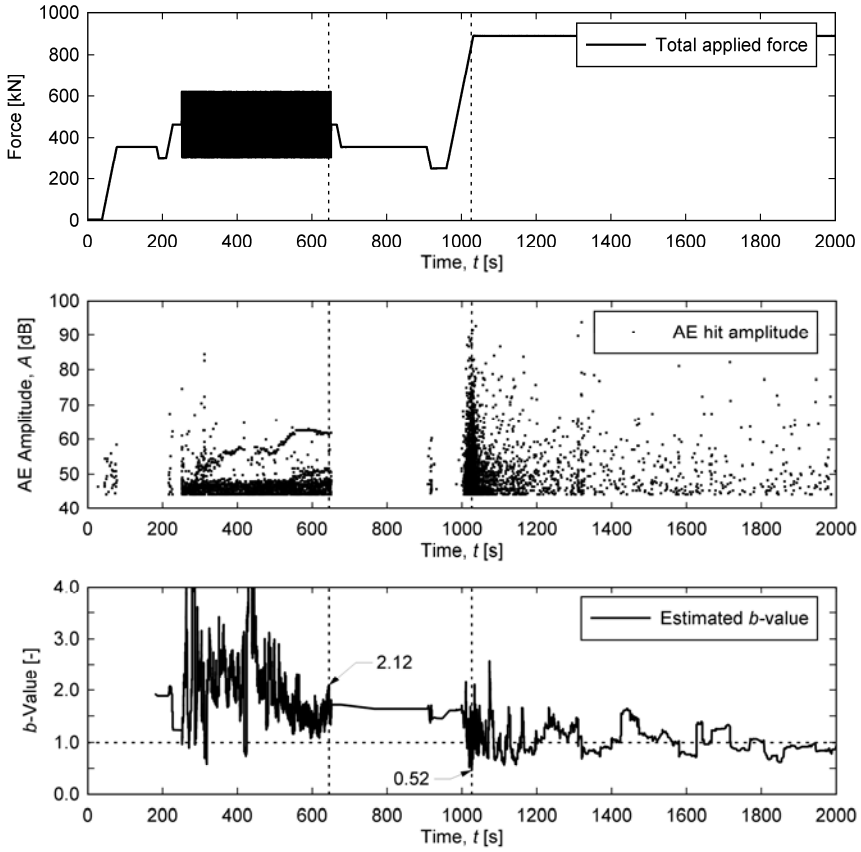

Fig. 3.9–Example of continuous *b*-value estimation for one sensor (from AE Specimen #2)

b-Value analysis appears especially well suited for implementation in a real-time Structural Health Monitoring (SHM) system because it is computationally inexpensive and, theoretically, only one sensor is needed to obtain a result. An example of such a continuous estimation of *b*-values is illustrated in Fig. 3.9 for the beginning of phase 2 for AE Specimen #2. The top figure shows the total applied force. The procedure starts with application of the dead load (356 kN (80 kips)), then cyclic loading (between 302 and 623 kN (68 and 140 kips)), followed by the overload (890 kN (200 kips)). The middle figure shows the resulting AE hit amplitudes over time. In the bottom figure, estimated *b*-values for sensor 4 are shown which was located on top of the web about 1.10 m away from the edge of the left bearing plate (see Fig. 3.3). The locations of the two individual *b*-values presented in Fig. 3.8 are indicated as well by vertical dotted lines in Fig. 3.9.

It can be observed that the obvious drop in the estimated *b*-value, which also represented the lowest value over the whole loading sequence, corresponds with the maximum applied force which caused propagation of existing cracks on the section. However, it was observed that *b*-value time histories differed from sensor to sensor. They appear to be a function of the sensor location with respect to the damage source location. It is therefore probably not meaningful to define an absolute critical *b*-value. Such critical values would have to be established during long term monitoring and parallel observation of structural performance.

One difference between AE in RC compared to seismic applications is that for the latter, attenuation of waves along the travel path is accounted for (Weiss 1997). As quantified by several authors (Landis and Shah 1995; Lovejoy 2006; Schumacher 2008; Uomoto 1987), attenuation in RC is quite significant and taking it into account could be used to improve *b*-value analysis. Future work may investigate this feature.

3.3.3 Proposed *Minimum b-Value Analysis*

For routine inspections of in-service bridges, a method called *Minimum b-Value Analysis* to quantify the effect of a passing vehicle on the monitored bridge component or section is proposed. As explained earlier, reductions in the *b*-value may indicate the localization of damage, i.e. macro-crack formation and propagation. This information may be used in conjunction with knowledge about the applied loading, i.e. passing vehicles (ambient or test trucks) to help estimate the current operating load level of a bridge component along with some information about the past lifetime loading history. The *Minimum b-Value* is determined by the following steps:

1. Determine lowest *b*-values from one complete load event for each of the AE sensors (defined by the test truck load effect)
2. Compute sensor network mean and standard deviation for all values obtained from step 1

For repeated load events of the same magnitude, *Minimum b-Values* are determined over all cycles, e.g. if there are three load cycles and eight sensors, the mean and standard deviation are taken over 24 estimated *b*-values.

Fig. 3.10 illustrates two examples of applied loads in the laboratory. The left and right figure show an applied overload (load that exceeds all maximum previous experienced loads) and a service-level load (load to be expected under everyday conditions), respectively. *b*-Values are shown as dashed lines and the total applied force as solid line with diamonds. For the examples in Fig. 3.10, the *Minimum b-Values* (and standard deviation) were 0.55 (0.06) and 1.33 (0.31) for the overload (OL) and the simulated test truck (TT), respectively. The approach presented in this paper intends to give an averaged representation of ongoing deterioration from within a region or section of interest, e.g. an existing crack or a cracked region.

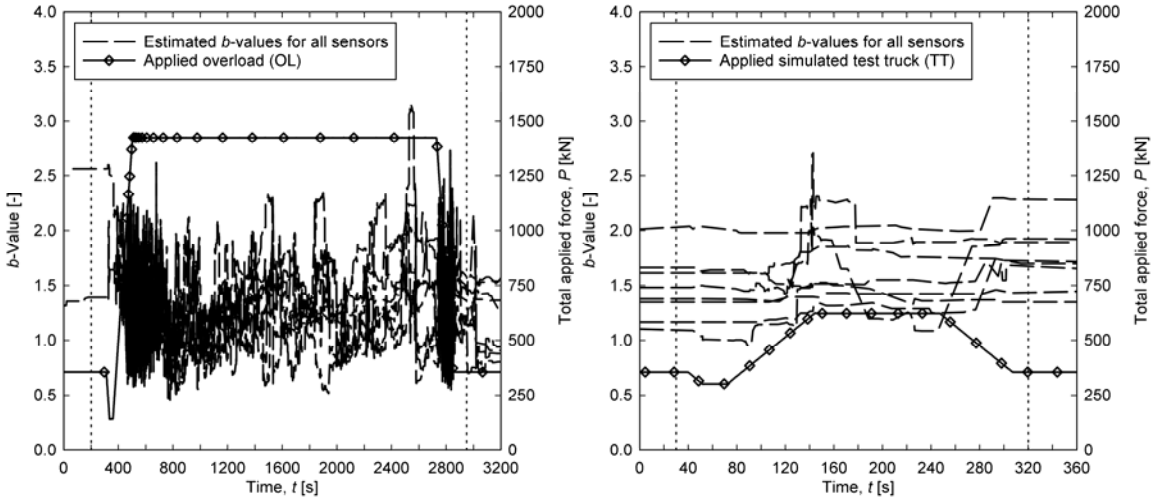

Fig. 3.10–Examples of continuous *b*-values for an overload (left Fig.) and a simulated test truck (right Fig.) over the course of one complete load cycle

3.3.4 *Minimum b-Values* from Laboratory Experiment

Presented and evaluated in this section are results from the proposed *Minimum b-Value Analysis* for the entire laboratory experiment including both AE Specimens. *Minimum b-Values* were estimated as introduced in section 3.3 with 50 consecutive AE hit amplitudes included in the computation. The AE data of both AE Specimens was then combined in all subsequent plots.

Fig. 3.11 shows two interesting aspects of the influence by the stage of deterioration on estimated *Minimum b-Values*. Linear curve-fits were computed over the *Minimum b-Values* of both specimens. Error bars represent one standard deviation for a set of estimated *b*-values. The left Fig. shows all applied overloads (OL), i.e. with force ratios *LR2* > 1.0. It can be observed that

those produce *Minimum b-Values* well below a value of 1.0, even below 0.5, which was suggested earlier by other researchers (Colombo et al. 2003; Kurz et al. 2006; Shiotani et al. 2000). Also, there is a visible overall trend for *Minimum b-Values* to decrease as ultimate capacity, i.e. *LR1* = 1.0, is approached. In the right figure, *Minimum b-Values* for the simulated 623 kN (140 kips) test trucks (TT) are plotted against the stage of deterioration (load phase), i.e. *LR3*. A trend for the *Minimum b-Value* to increase as the specimen has experienced higher loads in the past can be observed for that truck type, which is the most realistic one in terms of weight. This already implies that no absolute threshold for *Minimum b-Values* should be selected for interpretation of load effects. For some of the heavier test trucks (712 to 979 kN (160 to 220 kips)), there were too few data points generated to draw conclusions.

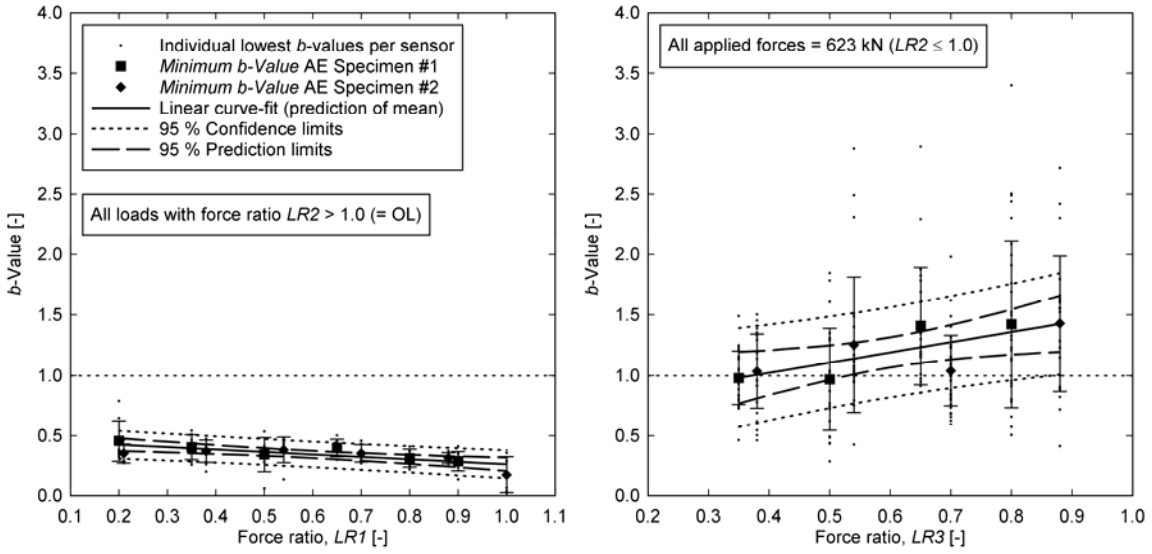

Fig. 3.11–*Minimum b-Values* for all overloads, i.e. *LR2* > 1.0 (left Fig.), and applied simulated 623 kN (140 kips) test trucks (right Fig.) for both AE specimens

Figs. 3.12 and 3.13 show estimated *Minimum b-Values* for both specimens for all simulated test trucks and overloads within the same load phase. Exponential curve-fits best represented the relationship and were computed over the *Minimum b-Values* of both specimens. Error bars represent one standard deviation for a set of same magnitude applied forces as listed in Table 3.1.

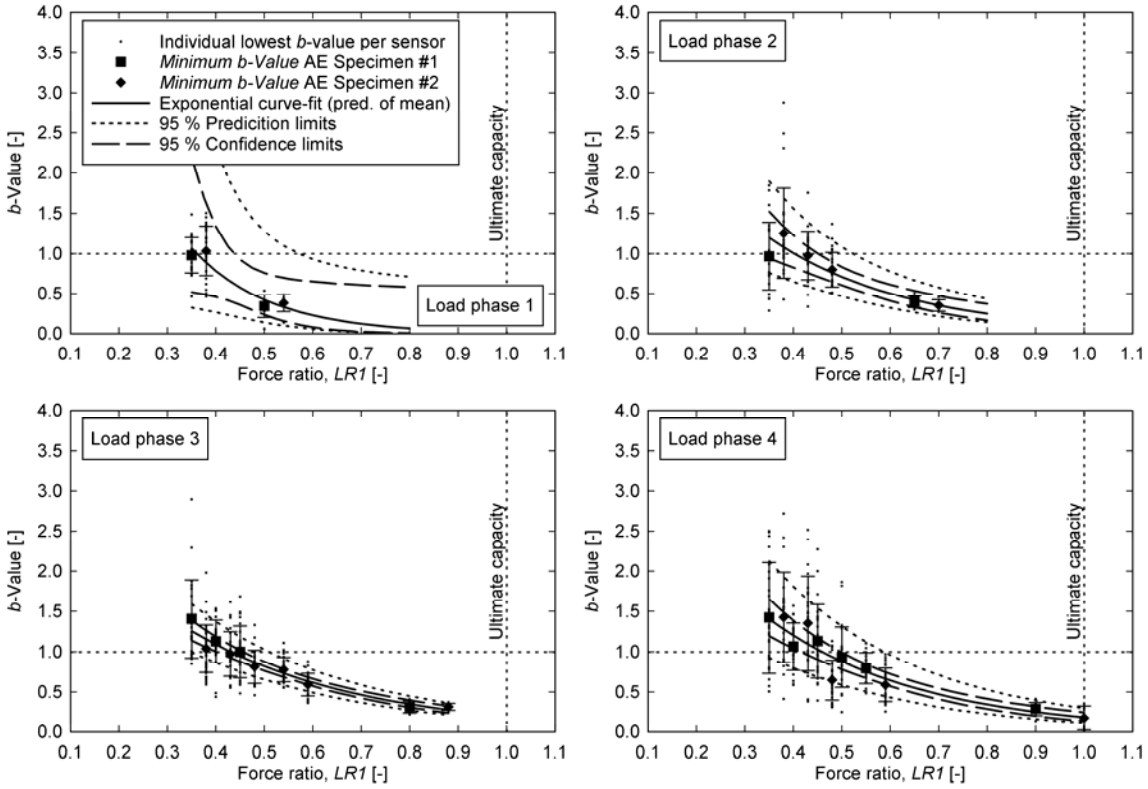

Fig. 3.12–Estimated *Minimum b-Values* for each load phase vs. load ratio *LR1*

Fig. 3.12 shows *Minimum b-Values* plotted against the force ratio *LR1* as presented in Eqn. 3.1 for each load phase. The ultimate capacity is shown as a vertical dotted line at *LR1* = 1.0. A clear trend can be observed for the *Minimum b-Value* which decreases with increasing force ratio *LR1*. Exponential least squares curve-fits over the *Minimum b-Values* produced squared correlation coefficients ranging between 91 and 97%. It can also be observed that the data variation (or scatter) decreases as the force ratio *LR1* increases, i.e. the 95% prediction limit bands become narrower which may be interpreted as damage becoming more localized also macro-cracking is occurring. The same trend was present for the error bars that represent the data variation of the individually applied loads.

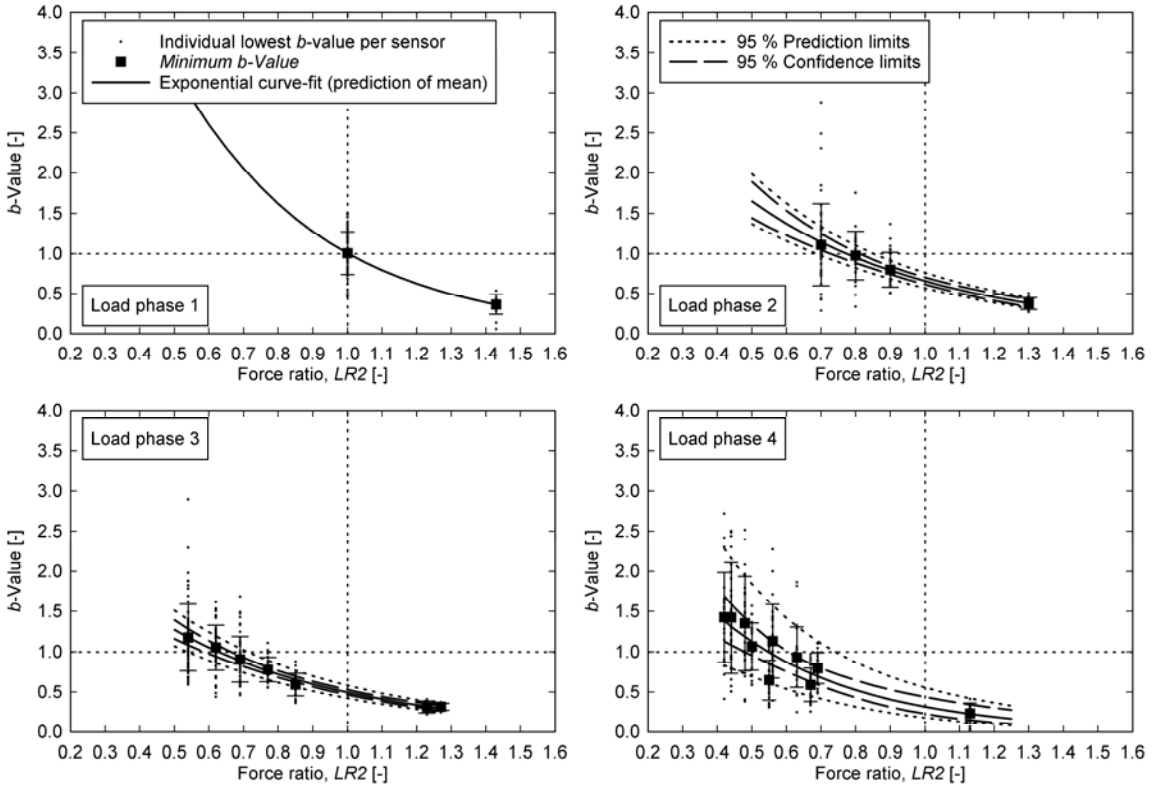

Fig. 3.13–Estimated *Minimum b-Values* for each load phase vs. load ratio *LR2*

In Fig. 3.13, *Minimum b-Values* are plotted against the force ratio *LR2* as defined in Eqn. 3.2. Each of the figures are divided into two parts by a vertical dotted line at *LR2* = 1.0 which is where the applied force is equal to the maximum previous applied force. *Minimum b-Values* with a force ratio *LR2* ≤ 1.0 and *LR2* > 1.0 represent applied TTs and OLs, respectively. An obvious trend is seen as the *Minimum b-Value* decreased with increasing applied loads during all load phases. Exponential least squares curve-fits produced squared correlation coefficients ranging between 89 and 99%. For load phase 1, there were only two data points available. The same exponential relationship found in the subsequent load phases was applied for that case. It can also be observed that the data variation (or scatter) decreases as the force ratio *LR2* increases, i.e. the 95% prediction limit bands become narrower, again, suggesting that damage was becoming more localized with macro-cracking occurring as an experienced previous maximum OL was reached or exceeded, i.e. *LR2* ≥ 1.0.

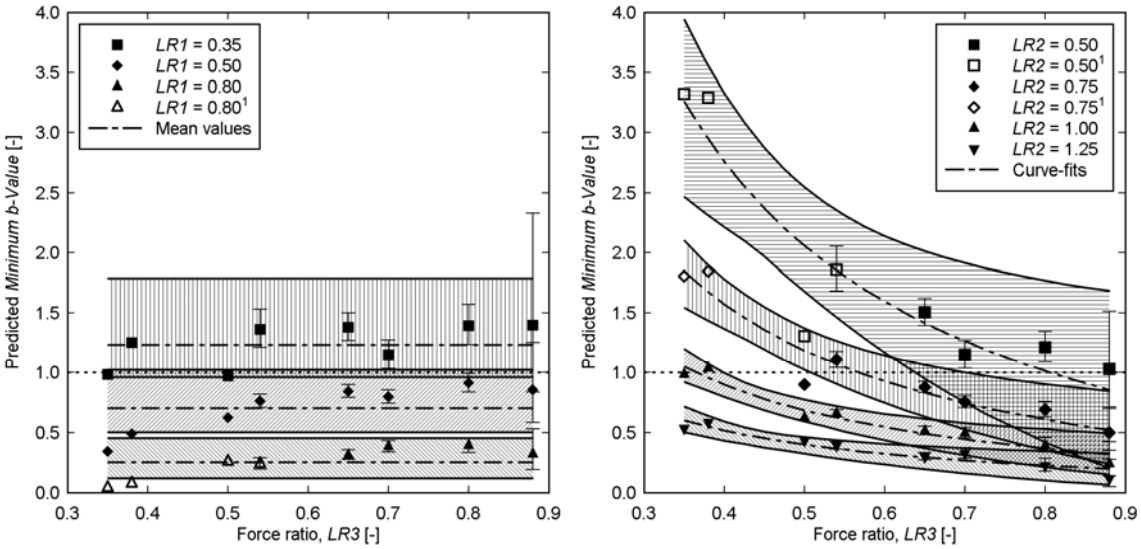

Fig. 3.14–Predicted *Minimum b-Values* for constant *LR1* (left Fig.), and constant *LR2* (right Fig.) for both AE specimens
[1] Extrapolated values

In Fig. 3.14, predicted *Minimum b-Values* for a few selected values of force ratios *LR1* (left figure) and *LR2* (right figure) are plotted against the force ratio *LR3* as introduced in 3.3. Both figures were constructed using predicted curve-fit mean data extracted from Figs. 3.12 and 3.13; error bands represent 95% confidence limits of those. The left figure shows the relationship that was found between estimated *Minimum b-Values* from simulated service level test trucks and their proximity to ultimate capacity. Three different values for the force ratio *LR1* were assumed over all load phases, i.e. simply the mean values were computed for each pre-selected *LR1* over the whole range of *LR3*. For the present full-scale laboratory specimens, a *Minimum b-Value* below 0.5 suggests the applied load was approximately equal to 80% (*LR1* = 0.80) of ultimate capacity of the specimen. *Minimum b-Values* between 0.5 and 1.0, and above 1.0 imply those were approximately equal to 50% and 35% of ultimate capacity, respectively. The right figure visualizes the relationship between current and previous applied forces and could hence be used to develop a tool to help estimate the operating load conditions of in-service bridges. It can be observed that this relationship is dependent on the stage of deterioration (or load phase). As an example on how to use this figure, consider the following. Assume an imposed force of 600 kN (135 kips) is applied using controlled test trucks. After applying that force, a *Minimum b-Value* of 2.0 is determined, based on AE monitoring (assumption). From the figure we can observe that that corresponds to a force ratio *LR2* of approximately 0.75. This means that the highest previous

force the element has experienced is approximately 600 kN/0.75 = 800 kN (135 kips/0.75 = 180 kips). For real bridges, the difficult part will be to determine the stage of deterioration, i.e. to estimate the force ratio *LR3*.

3.4 Conclusions

A new quantitative method to analyze AE data for estimation of the operating load level of a cracked RC bridge girder has been introduced. Two full-scale laboratory specimens with realistic geometry, material properties, and reinforcement detailing were tested. A sophisticated experimental test setup and loading protocol accounted for realistic loading conditions including simulation of ambient traffic. Simulated test truck weights were selected according to earlier in-service load tests and strain measurements (Potisuk and Higgins 2007). It was found that the proposed method called *Minimum b-Value Analysis* has the potential to estimate the load levels on operating RC bridge girders. The AE characterizing loading can be applied using heavily loaded maintenance trucks as was done for the in-service load test presented in Lovejoy (2006). It is important to recognize that structural sufficiency should never be drawn solely based on the evaluation of AE data but in conjunction with other physical measurements such as rebar strain or crack motion and detailed structural analyses and evaluations. AE sources from RC components can be many fold and the development and redistribution of stresses experienced during the life of a bridge are very complex. Additionally, external sources have to be expected that can produce high amplitude AE signals which can interfere with *b*-value computations (Schumacher et al. 2009). However, useful information can be gained by taking advantage of the proposed method. Based on the present work, the following observations and conclusions are made:

1. The main advantage of AE monitoring lies in real-time monitoring (example see Fig. 3.9) as overloads that occur are significantly bigger than experienced previous loads will be easily distinguishable. Such overloads will produce *b*-values well below 1.0, most likely even below 0.5 as shown in Fig. 3.11 (left).
2. Loads of the same magnitude, i.e. the 623 kN (140 kips) simulated test truck, produced higher *b*-values in later experimental phases where elevated visual distress (number of cracks and crack widths) was present as shown in Fig. 3.11 (right).
3. *Minimum b-values* decreased with higher applied forces (Figs. 3.12 and 3.13) even when the residual stresses have previously been removed by imposing cyclic loading until strains and displacements reach steady state. This has not been investigated previously in literature.
4. Scatter is higher for AE data compared to physical measurements. This is due to the irreversibility of AE, i.e. subsequent applied forces with the same magnitude tend to produce slightly lower *b*-values. It is recommended to perform several loadings of the

same magnitude to compute an average value. The variability of the computed *b*-values should always be reported as well.

5. Other physical measurements are crucial for comparison and verification of high amplitude AE signals that could otherwise be caused by other external sources, e.g. the noise caused by vehicles that are equipped with studded snow tires (Schumacher et al. 2009).
6. Events prior to the loading cycles of interest can still have an influence on the estimation of *b*-values because a certain number, e.g. 50 AE hit amplitudes back in time are required for the computation. It is thus, again, highly recommended that the imposed load be repeated several times to provide characteristic results rather than mixing with variable unknown traffic loading.
7. It is unreasonable to estimate the ultimate capacity of a bridge or component based solely on *Minimum b-values*. However, the technique could potentially provide insight into the operational load levels on the bridge by assuming a level of deterioration. This is visualized in Fig. 3.14 (right).

In a next step, AE data collected during an in-service load test (Lovejoy 2006) will be evaluated with the proposed *Minimum b-Value Analysis* and compared to the experimental results found in the present paper. Sensor type, sensor array geometry, and data acquisition settings were retained to facilitate comparison of results.

3.5 Acknowledgements

This work was carried out in the Structural Laboratory at Oregon State University as part of the research project SPR 633. The sponsorship and support by the Oregon Department of Transportation (ODOT) under the coordination of Mr. Steven M. Soltesz is greatly appreciated.

3.6 References

Carpinteri, A., Lacidogna, G., and Niccolini, G. (2006). "Critical Behaviour in Concrete Structures and Damage Localization by Acoustic Emission." *Key Engineering Materials*, 312, 305-310.

Carpinteri, A., Lacidogna, G., and Puzzi, S. (2009). "From criticality to final collapse: Evolution of the "b-value" from 1.5 to 1.0." *Chaos, Solitons & Fractals*, 41(2), 843-853.

Colombo, S., Main, I. G., and Forde, M. C. (2003). "Assessing Damage of Reinforced Concrete Beam Using "b-value" Analysis of Acoustic Emission Signals." *ASCE Journal of Materials in Civil Engineering*, 15(3), 280-286.

Cox, S. J. D., and Meredith, P. G. (1993). "Microcrack Formation and Material Softening in Rock Measured by Monitoring Acoustic Emissions." *International Journal of Rock Mechanics and Mining Sciences & Geomechanics Abstracts*, 30(1), 11-24.

Grosse, C. U., and Ohtsu, M. (2008). *Acoustic Emission Testing - Basics for Research-Applications in Civil Engineering*, Springer Verlag, Berlin & Heidelberg, Germany.

Gutenberg, B., and Richter, C. F. (1949). *Seismicity of the earth and associated phenomena*, Princeton University Press, Princeton, NJ.

Hardy, H. R., Jr. (1971). "Application of Acoustic Emission Techniques to Rock Mechanics Research." Symposium on Acoustic Emission at the ASTM Committee Meeting, Bal Harbor, FL.

Higgins, C. C., Miller, T. H., Rosowsky, D. V., Yim, S. C., Potisuk, T., Daniels, T. K., Nicholas, B. S., Robelo, M. J., Lee, A.-Y., and Forrest, R. W. (2004a). "Assessment Methodology for Diagonally Cracked Reinforced Concrete Deck Girders." Oregon Department of Transportation (ODOT), Salem, OR.

Higgins, C. C., Yim, S. C., Miller, T. H., Robelo, M. J., and Potisuk, T. (2004b). "Remaining Life of Reinforced Concrete Beams with Diagonal-Tension Cracks." Oregon Department of Transportation (ODOT), Salem, OR.

Kuennen, T. (2006). "Taming Oregon's Cracked Bridges." Better Roads, Randall-Reilly Publishing Co., Des Plaines, IL, 54-63.

Kurz, J. H., Finck, F., Grosse, C. U., and Reinhardt, H.-W. (2006). "Stress Drop and Stress Redistribution in Concrete Quantified Over Time by the b-value Analysis." *Structural Health Monitoring*, 5(1), 69-81.

Landis, E. N., and Shah, S. P. (1995). "Frequency-Dependent Stress Wave Attenuation in Cement-Based Materials." *ASCE Journal of Engineering Mechanics*, 121(6), 737-743.

Lovejoy, S. C. (2006). "Development of Acoustic Emissions Testing Procedures Applicable to Convetionally Reinforced Concrete Deck Girder Bridges Subjected to Diagonal Tension Cracking," PhD Dissertation, Oregon State University, Corvallis, OR.

Miller, R. K., Hill, E. v. K., and Moore, P. O. (2005). *Nondestructive Testing Handbook - Volume 6 - Acoustic Emission Testing*, American Society for Nondestructive Testing (ASNT), Columbus, OH.

Pollock, A. A. (1981). "Acoustic Emission Amplitude Distributions." International Advances in Nondestructive Testing, 215-239.

Potisuk, T., and Higgins, C. C. (2007). "Field Testing and Analysis of CRC Deck Girder Bridges." *ASCE Journal of Bridge Engineering*, 12(1), 53-63.

Rao, M. V. M. S., and Prasanna Lakshmi, K. J. (2005). "Analysis of b-value and improved b-value of acoustic emissions accompanying rock fracture." *Current Science*, 89(9), 1577-1582.

Rundle, J. B., Turcotte, D. L., Shcherbakov, R., Klein, W., and Sammis, C. (2003). "Statistical Physics Approach to Understanding the Multiscale Dynamics of Earthquake Fault Systems." *Reviews of Geophysics*, 41(4), 5.1-5.30.

Schumacher, T. (2008). "Acoustic Emission Techniques Applied to Conventionally Reinforced Concrete Bridge Girders." Oregon Department of Transportation (ODOT), Salem, OR.

Schumacher, T., Higgins, C. C., and Lovejoy, S. C. (2009). "Detection of Studded Tires Using Acoustic Emission Sensors Mounted to Highway Bridges." *ASCE Journal of Transportation Engineering*(accepted for publication on 04/24/2009).

Shiotani, T., and Ohtsu, M. (1998). "Prediction of Slope Failure Based on AE Activity." Acoustic Emission: Standards and Technology Update, ASTM STP 1353, American Society for Testing and Materials, 156-171.

Shiotani, T., Yuyama, S., Li, Z. W., and Ohtsu, M. (2000). "Quantitative Evaluation of Fracture Processes in Concrete by the Use of Improved b-Value." Non-Destructive Testing in Civil Engineering 2000 (Seiken Symposium No. 26), Elsevier, Tokyo, Japan, 293-302.

Stein, S., and Wysession, M. (2003). *An Introduction to Seismology, Earthquakes, and Earth Structure*, Blackwell Publishing Ltd., Malden, MA.

Uomoto, T. (1987). "Application of Acoustic Emission to the Field of Concrete Engineering." *Journal of Acoustic Emission*, 6(3), 137-144.

Weiss, J. (1997). "The Role of Attenuation on Acoustic Emission Amplitude Distributions and b-Values." *Bulletin of the Seismological Society of America*, 87(5), 1362-1367.

Estimation of Acoustic Emission Source Locations: A Bayesian Approach

Thomas Schumacher, Daniel Straub, Christopher C. Higgins

Journal of Sound and Vibration
Elsevier B.V.
Customer Service Department
3251 Riverport Lane
Maryland Heights, MO 63043
USA

To be submitted.

4 Third Manuscript

Estimation of Acoustic Emission Source Locations: A Bayesian Approach

Thomas Schumacher[1], Daniel Straub[2], and Christopher C. Higgins[3]

Abstract: Acoustic Emissions (AE) are stress waves initiated by sudden strain releases within a solid body. These can be caused by internal mechanisms such as crack opening or propagation, crushing, or rubbing of crack surfaces. One application for the AE technique in the field of Structural Engineering is Structural Health Monitoring (SHM). With piezo-electric sensors mounted to the surface of the structure, stress waves can be detected, recorded, and stored for later analysis. An important step in quantitative AE analysis is the estimation of the stress wave source location. Commonly, source location results are presented in a purely deterministic manner as spatial and temporal points, excluding information about uncertainties and errors. Due to variability in the material properties and uncertainty in the mathematical model, measures of uncertainty are needed beyond best-fit point solutions for source locations. This paper introduces a framework for the development of a probabilistic source location algorithm using Bayesian analysis methods with Markov Chain Monte Carlo (MCMC) simulation where all source location parameters are described with a posterior probability density function (PDF). The proposed methodology is applied to an example employing data collected from a realistic section of a reinforced concrete bridge column. The selected approach is general and has the advantage that it can be extended and refined efficiently. Results are discussed and future steps to improve the algorithm suggested.

Keywords: Stress waves, Probabilistic source location algorithm, Parameter estimation, Bayesian analysis, Markov Chain Monte Carlo simulation.

[1] Graduate Research Assistant, School of Civil and Construction Engineering, Oregon State University, USA, E-mail: schumact@engr.orst.edu

[2] Associate Professor, Civil and Environmental Engineering, Technical University Munich, Germany, E-mail: straub@era.bv.tum.de

[3] Professor, School of Civil and Construction Engineering, Oregon State University, USA, E-mail: chris.higgins@oregonstate.edu

4.1 Introduction

4.1.1 Background on Acoustic Emission

Acoustic Emission (AE) is the *term used for transient elastic waves generated by the release of energy within a material or by a process* (EN 2000). A stress wave is generated, traveling from the source origin away to the surface of the body where it can be recorded by sensors. This process is irreversible and therefore not repeatable. Other terms include stress wave emission or nano-seismic activity. Within the family of non-destructive testing methods, AE has its own special place because it is a passive technique. AE are stress waves produced by a spontaneous internal dynamic process such as e.g. crack initiation or formation or internal material fracture. The source location and mechanism is therefore unknown and subject of our investigation. An introduction to the many applications in AE monitoring can be found in Grosse and Ohtsu (2008). Subsequently, the terms Acoustic Emission (or AE) and stress wave are used interchangeably.

In infinite elastic solids, two types of waves, sometimes referred to as modes, exist. The first is called compression, or primary (*p*-), wave where the particles move in the direction of the wave. The second is called shear, or secondary (*s*-), wave with particle motion perpendicular to the direction of the propagating wave. With the introduction of boundaries, a third wave type, the surface, or Rayleigh (*R*-) wave exists. Between the three wave mode velocities, c_p, c_s, and c_R, the following relationship is true (Graff 1991):

$$c_p > c_s > c_R \tag{4.1}$$

For locating sources, typically only the *p*-waves are of interest because they represent the first, undisturbed arrival of a stress wave. The *p*-wave velocity in an isotropic, homogeneous and elastic body can be determined as

$$c_p = \sqrt{\frac{E}{\rho}}\sqrt{\frac{1-\nu}{(1+\nu)(1-2\nu)}} \tag{4.2}$$

where E is the dynamic Modulus of Elasticity in N/m^2, ρ the material density in kg/m^3, and ν Poisson's Ratio (Graff 1991). Typical average values for the *p*-wave velocity and Poisson's Ratio

in reinforced concrete range from approximately $3.5 \leq c_p < 4.5$ m/ms ($140 \leq c_p < 180$ in./ms) and $0.25 \leq \upsilon < 0.30$, respectively (Schumacher 2008).

Stress waves emitted from AE sources are usually recorded by a network of piezo-electric sensors mounted to the surface of the specimen. These sensors are typically sensitive for frequencies ranging from approximately 10 to 500 kHz to capture the transient stress waves. The analog signal is intensified by an amplifier and digitized to enable hard disk storage. AE data is normally not acquired continuously, since that would produce enormous data files which would be difficult to analyze and interpret. Instead, pre-selected criteria are used to trigger the system for individual burst signals from which *p*-wave arrival times as well as qualitative wave form parameters are then extracted (Grosse and Ohtsu 2008).

The first important step in quantitative AE analysis is the estimation of spatial and temporal parameters of the stress wave source. If at least four sensors detect a discrete stress wave signal it can be identified as an event and the location and time of the source can be estimated. An AE event is defined as the *physical phenomenon giving rise to acoustic emission* (EN 2000). Fig. 4.1 illustrates a typical recorded transient stress wave signal recorded at sensor *k*. The first arrival of the stress wave, or *p*-wave arrival time, is enlarged and stretched in time for better clarity. The source occurrence time is unknown and denoted as t_0. For the arrival time of the *p*-wave, two values are shown: $t_{a[k],man}$ denotes the arrival time picked manually, and $t_{a[k],auto}$ by some automated picking method. *A* denotes the maximum signal amplitude. Depending on the method employed, an error Δt will be inherent in the detected arrival times and is often unavoidable.

The first crucial step in reliable AE source location estimation is the accurate determination of the *p*-wave arrival times from each sensor in the network. A picker based on the Akaike Information Criterion (AIC) was employed as presented in Kurz et al. (2005). This method has proven reliable and accurate in picking arrival times from stress waves (Schechinger 2006).

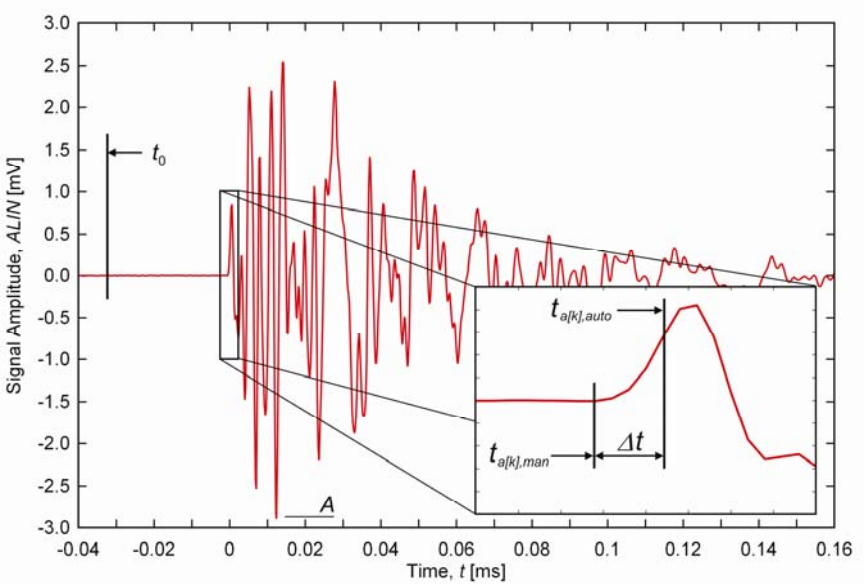

Fig. 4.1–AE burst signal example with enlarged *p*-wave arrival at sensor *k*

4.1.2 Source Location Algorithms

Traditional Deterministic Methods

Traditional methods shall be defined as deterministic methods that do not take into account variability of parameters, i.e. location of sensors, *p*-wave velocity, arrival times, etc. are assumed as constants. If the source hypocenter and sensors are modeled as dimensionless points and the travel path of the stress wave is assumed as a straight line between source and sensor, and the *p*-wave velocity c_p assumed as constant and known for all travel paths, the following general relationship, sometimes referred to as *arrival time function*, for one event can be derived:

$$f(x_0, y_0, z_0, t_0) = t_{a[k]} = t_0 + \frac{d_{[k]}}{c_p} \tag{4.3}$$

where t_0 is the event source time and x_0, y_0, and z_0 are the event source coordinates. The signal travel distance $d_{[k]}$ between source and sensor locations is calculated as

$$d_{[k]} = \sqrt{(x_{[k]} - x_0)^2 + (y_{[k]} - y_0)^2 + (z_{[k]} - z_0)^2} \tag{4.4}$$

The Cartesian coordinates of sensor k are denoted with $x_{[k]}$, $y_{[k]}$, and $z_{[k]}$. To solve for the four unknowns x_0, y_0, z_0, and t_0, time arrivals $t_{a[k]}$ from at least four sensors must be detected. Most commonly, this non-linear inverse problem is solved by employing iterative algorithms based on Geiger's method (Geiger 1910). A summary of existing deterministic schemes can be found for example in Ge (2003a; Ge 2003b). These algorithms provide a covariance matrix of source coordinates as an estimate of uncertainty if arrival times from at least five sensors are available. Fig. 4.2 shows an example of three estimated locations (from the same calibration experiment used for this study presented in section 4.1.3) employing a traditional deterministic source location scheme implemented by the author (Schumacher 2008). Mean solutions are shown at the center of the red pentagrams; red, blue, and green lines represent first, second, and third principal standard deviations σ_1, σ_2, and σ_2, respectively, that were computed from the covariance matrix. The grey cross marks the actual location of the initiated stress wave source and yellow circles represent the sensors (with numbers in parentheses).

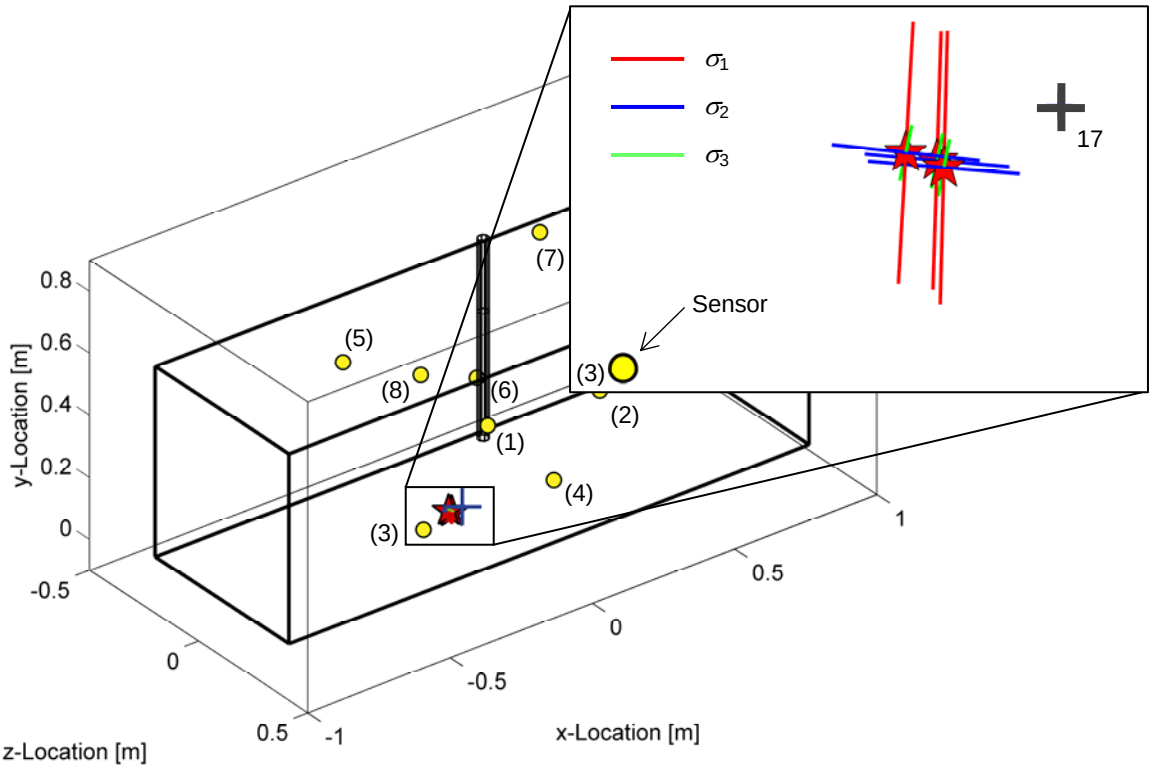

Fig. 4.2–Example of three estimated locations from a known source using a traditional scheme

It can be observed that bias (off-set of the mean estimated solution to the known source location) and variance are both present in the estimated source locations. It appears that the standard deviations indicating the location uncertainty do not properly reflect these errors. This deterministic approach does not account for all intrinsic uncertainties and errors in the model and systematic errors can only be detected when the true source location is known, which is usually not the case for AE applications.

Probabilistic Approaches

A paper that is useful in the context of this study was written by Tarantola and Valette (1982). It describes how inverse problems like hypocenter locations of earthquakes can be stated using random variables and distribution parameters to describe uncertainties in the arrival time picking using a Bayesian approach. An example is given, assuming sensor locations as well as wave velocity are deterministic. The authors suggested using PDFs to describe parameters rather than simple central point estimators. This worked well for their relatively simple example where all parameters were assumed with a normal distribution so an analytical solution could be computed. All uncertainties are basically lumped into one. At the time of development, powerful optimization algorithms were not readily available.

In earthquake source location, probabilistic methods have been employed for a number of years (Lomax et al. 2000; Tarantola and Valette 1982). Based on these methods, a first approach to account for the probabilistic nature of AE source parameters was undertaken by Schechinger (2006). In their work, an adapted version of a computer program called *NonLinLoc* was used. This program was originally developed by Lomax (2008) for the estimation of earthquake epicenter locations and computes a posterior probability density function (PDF) by Monte Carlo (MC) simulation using importance sampling taking into account model and parameter uncertainties (Lomax et al. 2000). The maximum likelihood point of the posterior distribution is used as optimal source location. Non-homogeneous material models that allow the existence of a non-linear velocity field can be implemented as well. A comparison of four different AE events located with *NonLinLoc* and a traditional scheme that was extracted from Schechinger (2006) is illustrated in Fig. 4.3. Shown is part of a concrete specimen section containing an air void that represents a prestressing duct.

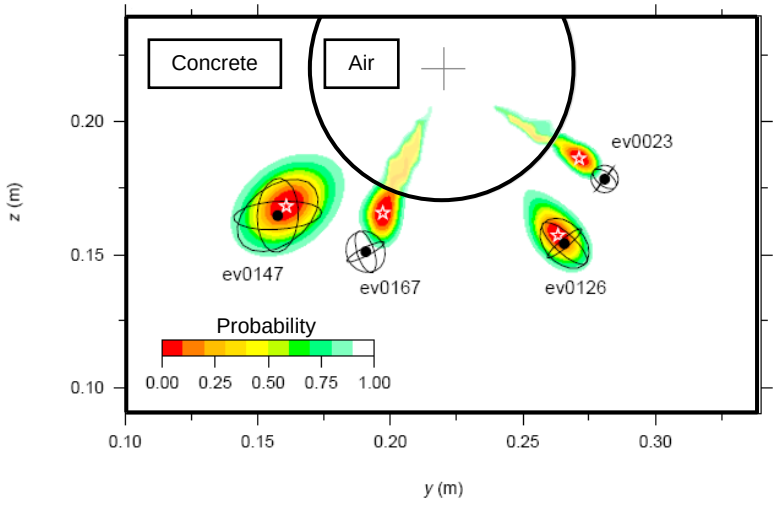

Fig. 4.3–Comparison of different source location schemes, graph (modified) from Schechinger (2006)

It can be observed that for events ev0023 and ev0167, the maximum likelihood point of the posterior distribution (white pentagram) differs from the point-estimate (black filled circle). Also, the posterior PDF (colored areas) is different from the uncertainty estimate provided by the traditional algorithm (ellipsoids). This is explainable by the fact that these two events are relatively close to the void (air) and their estimation is therefore more affected by the slow velocity in that region. On the other hand, there is only a relatively minor difference between the two solutions for events ev0126 and ev0147.

Wéber (2006) used the same program as Schechinger, *NonLinLoc* (Lomax 2008), to retrieve hypocenter location and source time function data from weak seismic events. The a priori PDF is estimated by the arrival times of the sensor network with the covariance matrix. The final hypocentral location is described as the mode of the a posteriori PDF. Obviously, here as well parameter uncertainties are estimated theoretically based on the wave forms only and assume a Gaussian distribution.

Tarantola and Valette (1982) suggested the use of Bayes' theorem to obtain posterior PDFs for the spatial source location parameters. This is realized in the program *NonLinLoc* (Lomax 2008).

The approach chosen for the present work was that posterior distributions for all model parameters are first estimated using a large data set of observed arrival times. These estimated parameters are then used in conjunction with a predictive algorithm to create complete spatial as well as temporal posterior PDFs for the source location parameters.

4.1.3 Experiment Used for this Study

A calibration experiment was performed on this specimen prior to the load test using pencil lead breaks (PLB) applied to the surface of the specimen (Schumacher 2006). Five individual PLB to initiate stress waves were performed on 76 x 76 mm (3 x 3 in.) grids on the front *x*-*y* and top *x*-*z* face, and the bottom of the pull-out rebar, and are shown as grey crosses in Fig. 4.4. PLB represent a common means to produce highly repeatable stress wave sources in AE (EN 2000). Eight AE sensors were deployed non-symmetrically on four faces of the specimen and are shown as yellow cylinders. Sensor location coordinates are listed in Table 4.1.

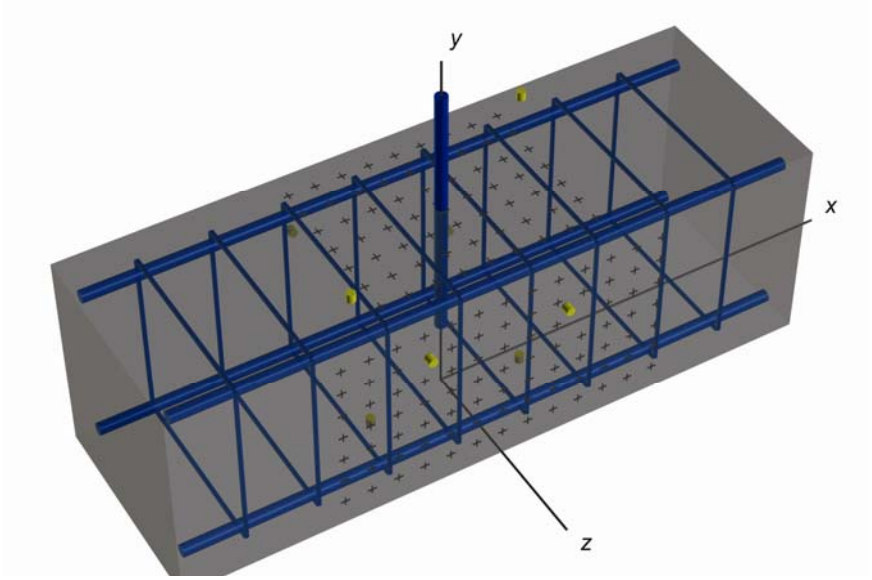

Fig. 4.4–View of reinforced concrete test specimen with all PLB locations (specimen is semi-transparent to visualize embedded reinforcing bars)

The test specimen was a full-scale reinforced concrete section of a bridge bent cap column with dimensions l_z x l_y x l_x = 610 mm x 610 mm x 1.83 m (24 in. x 24 in. x 6 ft). This specimen was originally designed to determine the ultimate anchorage force of the embedded ø 35 mm (#11) reinforcing bar aligned with the *y*-axis (Koester 2007). The embedment length of this bar was 406

mm (16 in.). Other steel reinforcing bars are shown for reference. All reinforcing bars were Grade 60 (f_y = 414 MPa) and the average concrete compressive strength was found to be 28.0 MPa (4060 psi).

Table 4.1–Sensor locations

Sensor	*x*		*y*		*z*		Location	SE150-M
[-]	[mm]	[in.]	[mm]	[in.]	[mm]	[in.]	[-]	Serial #
1	-216	-8.5	457	18.0	302	11.9	front *x*-*y*	930
2	178	7.0	432	17.0	302	11.9	front *x*-*y*	940
3	-229	-9.0	0	0.0	25	1.0	bottom *x*-*z*	1221
4	229	9.0	0	0.0	25	1.0	bottom *x*-*z*	1250
5	-254	-10.0	394	15.5	-311	-12.3	back *x*-*y*	1254
6	216	8.5	178	7.0	-311	-12.3	back *x*-*y*	1259
7	394	15.5	613	24.1	-254	-10.0	top *x*-*z*	4202
8	-356	-14.0	613	24.1	178	7.0	top *x*-*z*	4203

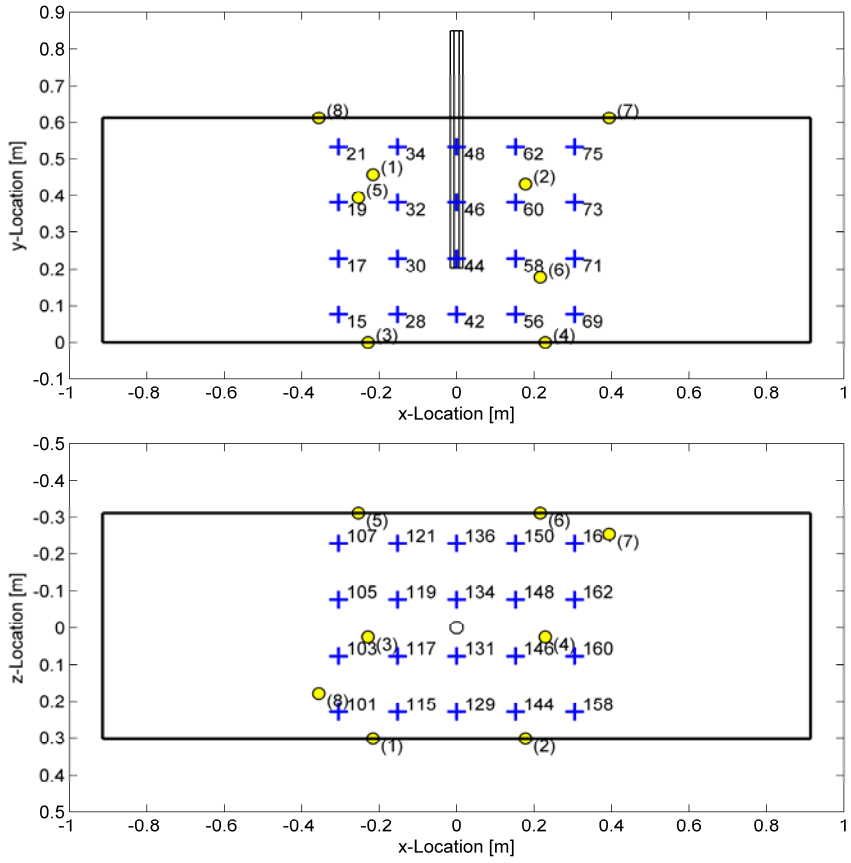

Fig. 4.5–PLB locations on specimen surface included in parameter estimation

To keep the amount of data to a reasonable limit, only 40 selected locations were included in the regression analysis and are shown in Fig. 4.5. The total number of observed arrival times included is: 40 locations x 5 PLB per location x 8 sensors = 1600 arrival times. The locations that lie on the front *x*-*y* face are numbered 15 to 75, the ones on the top *x*-*z* face 101 to 164. The sensors are shown as yellow circles.

4.2 Statistical Modeling Using Bayesian Analysis Methods

4.2.1 Concepts of Bayesian Analysis

Bayesian statistics, specifically the Bayesian updating formula, represent the main framework for incorporating uncertainties and errors in the present problem. The formula is based on the original Bayesian updating rule which states that for two events *A* and *B*,

$$P(A|B) = \frac{P(B|A)}{P(B)} P(A) \tag{4.5}$$

where $P(A|B)$ is the (updated) posterior probability of event *A* incorporating the knowledge that event *B* has occurred; $P(B|A)$ is the likelihood or probability of event *B* if *A* were to occur; $P(A)$ is the probability of the event *A* before knowledge about occurrence of *B*, also called prior probability; $P(B)$ represents a normalizing scalar. This rule can now be extended and applied for a random variable *X* having the PDF $f_X(x|\theta)$ with distribution parameters θ. In order to account for uncertainties in θ, it is considered a random variable Θ. Once events are observed that provide information about the random variable *X*, this new knowledge can then be used to update the distribution of Θ by using Eqn. 4.5 as follows:

$$f_\Theta(\theta|x) = \frac{L(\theta|x)}{c} f_\Theta(\theta) \tag{4.6}$$

where $f_\Theta(\theta|x)$ represents the posterior distribution conditioned on observation of outcomes of the random variable *X*, $L(\theta|x) = f_X(x|\theta)$ is the likelihood function of parameters θ for observed realizations of *x*, *c* a normalizing constant defined as the *m*-fold integral $\int_{-\infty}^{\infty} \dots \int_{-\infty}^{\infty} L(x|\theta)\, p_\Theta(\theta)\, d\theta_1 \dots d\theta_m$ where *m* is the number of parameters, and $f_\Theta(\theta)$ the prior distribution for Θ before additional knowledge is gained.

Once the posterior distribution $f_\Theta(\theta \mid x)$ for the parameters is obtained, it can be incorporated in a general predictive joint distribution of the form

$$f_Y(y \mid x,\theta) = \int_{-\infty}^{\infty} \dots \int_{-\infty}^{\infty} f_Y(y,\theta) f_\Theta(\theta \mid x) d\theta_1 \dots d\theta_m \tag{4.7}$$

to predict future events *Y* based on knowledge from past observed realizations *x* and estimated parameters θ. The difficulty lies in computing the integrals in Eqns. 4.6 and 4.7, for which analytical solutions exist only in special cases. Numerical methods using Monte Carlo (MC) simulation techniques represent a powerful means to address this problem and are introduced in the following section.

4.2.2 The Numerical Approach

The computer program utilized for the present work is called *WinBUGS* and available free for download (Imperial College and Medical Research Council 2007). This program enables Bayesian inference and numerical analysis of complex data using Markov Chain Monte Carlo (MCMC) simulation techniques. An introduction to this field can be found in Gilks et al. (1996) as presented in section 4.2.1. That problem is greatly simplified and generalized by using MCMC. For instance, integrations become simple summations and expectations simple averages of a collection of random samples drawn from specified distributions in the correct proportions. This is of course an approximation process as the population mean μ for example is estimated by a sample mean $\bar{x}$. Large numbers of samples, however, will ensure desired accuracy. A Markov Chain is a sequence of computations where the next step only depends on the current step, but not on any earlier steps in time, i.e. $X_{t+1} = f(X_t)$. The intent is that, eventually, the chain will become independent of its initial (or prior) state, and gradually converge to a unique stationary (posterior) state that does neither depend on the time step *t* nor the initial state X_0. The sampling of X_{t+1} conditioned on X_t is based on the Gibbs sampling technique, a special form of the Metropolis-Hastings algorithm (Gilks et al. 1996).

4.2.3 Model and Parameter Uncertainties

Any mathematical model of a physical phenomenon includes uncertainties and comes with inherent errors as the true nature of a problem and its parameters are known only to a certain degree. The same is true for the present problem. For example, the specimen is assumed to be isotropic and homogeneous, but reinforced concrete is a composite material consisting of cement, aggregates, and embedded reinforcing steel, each constituent having significantly different wave propagation properties. And even if a non-uniform velocity model were considered, there would still be variability in each material property and corresponding uncertainty. However, numerical simulation of wave propagation has shown that typical reinforcing bar diameters do not change the stress wave propagation significantly (Schechinger 2006).

Fig. 4.6 shows a generic test specimen and visualizes the most important parameters involved in estimating stress wave source locations. Indices are assigned as follows and impose a distinct hierarchy in the model:

- *i* for pencil break locations (1 to 40)
- *j* for the event at each location (1 to 5)
- *k* for the sensors (1 to 8)

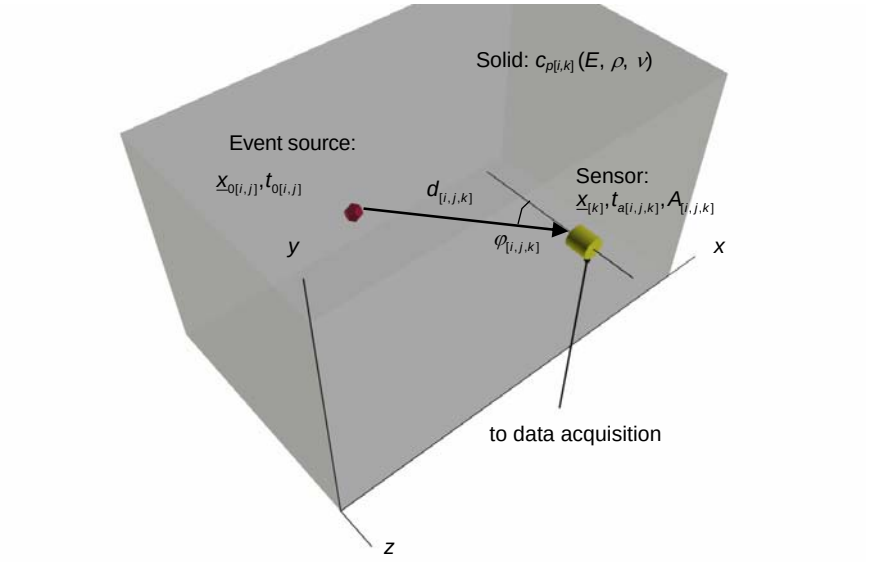

Fig. 4.6–Generic test specimen with parameters (only one sensor shown for clarity)

In Table 4.2, the most important parameters and an attempt to classify their variability into epistemic (*epi*) or aleatory (*ale*) uncertainty was undertaken (DerKiureghian 2001). Epistemic uncertainties are those associated with limited knowledge of the problem. They can be decreased by for example refining the mathematical model or gathering more information about a process. Aleatory uncertainties arise because of the inherent randomness in a system and are irreducible. These include for instance material properties that were determined through sample tests. The parameters in Table 4.2 were ranked subjectively, according to their importance based on experience and observation.

From a Bayesian point of view, there is no fundamental difference between these variable types, i.e. they are all regarded and treated as random quantities. However, it is still important to know which model parameters are present and irreducible and which can be influenced by improving the mathematical model or including more observations.

Table 4.2–Most important parameters present in source location estimations

Parameter	Type	Description
p-Wave arrivals, $t_{a[i,j,k]}$	*epi*	Accuracy of determination dependant on: - Signal-to-noise ratio of recorded signal - Wave travel path and attenuation characteristics Arrival time picking errors Δt may be a function of: - Wave travel path length, $d_{[i,j,k]}$ - Wave incident angle, $\varphi_{[i,j,k]}$ - Maximum signal amplitude, $A_{[i,j,k]}$ (observed)
p-Wave velocity, $c_{p[i,k]}$	*ale*	Function of material properties, micro-cracks: - Modulus of Elasticity, E - Material density, ρ - Poisson's Ratio, ν
Wave travel path, $d_{[i,j,k]}$	*ale/ epi*	Can deviate from straight line due to macro-cracks, voids, specimen geometry, etc.
Sensor locations, $x_{[k]}$	*epi*	Measurement errors, inexact placement
Source characteristics	*ale*	Type, spatial and temporal dimensions
Location scheme	*epi*	- Sensitivity of location with respect to sensors - Errors in the source location scheme
Sensor characteristics	*epi*	Sensitivity, resonant behavior

4.3 Model Formulation and Implementation

The development of a probabilistic stress wave source location algorithm to predict source location parameters in full probabilistic form based on Bayesian analysis concepts consists of the following steps:

1. Formulation of inference model
2. Estimation of model parameters using Bayesian inference
3. Implementation of predictive model
4. Model validation

In the succeeding four sections, these steps are described in detail.

4.3.1 Formulation of Inference Model

Based on the uncertainties described in section 4.2.3, a basic probabilistic model for the estimation of stress wave source locations was developed. The general relationship between source parameters and sensors is the arrival time function as stated in Eqn. 4.3 and visualized in Fig. 4.6. This function now restated taking into account uncertainties in the model parameters and errors. The slowness s_p was used as the descriptor for the motion of the *p*-wave rather than velocity c_p and is defined as:

$$s_p = c_p^{-1} \tag{4.8}$$

This was done in order to facilitate linear behavior of the probabilistic model during the inference process, so that the central model equation took the general form:

$$y = \beta_0 + \beta_1 x + \delta \tag{4.9}$$

In the present study, y represented the observed arrival times t_a, β_0 the event time t_0, β_1 the wave slowness s_p, and x the signal travel distance d. δ is a correction term that can be included to account for measurement uncertainty. Given the structure of the used data, the probabilistic model was assumed a multi-hierarchical, random effects type.

Variability in the model was assumed to be associated with the basic source location parameters which are the *p*-wave slowness s_p, the observed arrival times t_a, and the event time t_0. Note that not all parameters vary with each index *i*, *j*, *k*. There is only one event time t_0 per event, i.e. for a group of eight sensors, and thus it does not vary with *k*. The wave propagation characteristics were assumed to be the same for each PLB at a specific location and s_p therefore not updated with *j*. The travel distance *d* was assumed as deterministic and calculated from the 'known' source and sensor locations using Eqn. 4.4. The model equation is based on Eqn. 4.3 and can be stated as follows:

$$t_{a[i,j,k]} = t_{0[i,j]} + s_{p[i,k]} d_{[i,j,k]} \tag{4.10}$$

The corresponding probabilistic model can be written as:

$$T_{a[i,j,k]} \sim \mathrm{N}\left(t_{0[i,j]} + s_{p[i,k]} d_{[i,j,k]}, \tau_{t_a[k]}\right) \tag{4.11}$$

The parameters that were estimated and used to predict future events are the following:

- Mean *p*-wave slowness, μ_{s_p}
- Precision of the *p*-wave slowness, τ_{s_p}
- Precision of the observed arrival times, $\tau_{t_a[k]}$

The first two parameters are global parameters, i.e. not varying with any of the indices *i*, *j*, or *k*. Because uncertainty in the observed arrival times t_a was assumed to be associated to some degree with each sensor location, the precisions τ for the observed time arrivals were updated with *k*. The precision τ is defined as the inverse of the variance σ^2, where σ is the standard deviation:

$$\tau = \sigma^{-2} \tag{4.12}$$

All elements (in *WinBUGS* called nodes) used to describe a probabilistic model can be classified as stochastic, constant, or logical. *WinBUGS* allows for graphical representation of probabilistic

models which is illustrated in Fig. 4.7. Stochastic nodes require specification of prior distributions as described in section 4.2.1 and are listed in Table 4.3. Generally, Normal (N) distributions were assigned as priors to nodes that represented means and Uniform (U) distributions as priors to nodes that represented standard deviations.

A correction term δ was not included in the model at this point. This is planned for future work and may be used to employ additional information such as the signal strength or the angle at which the stress wave arrives at the sensor to enhance the probabilistic model.

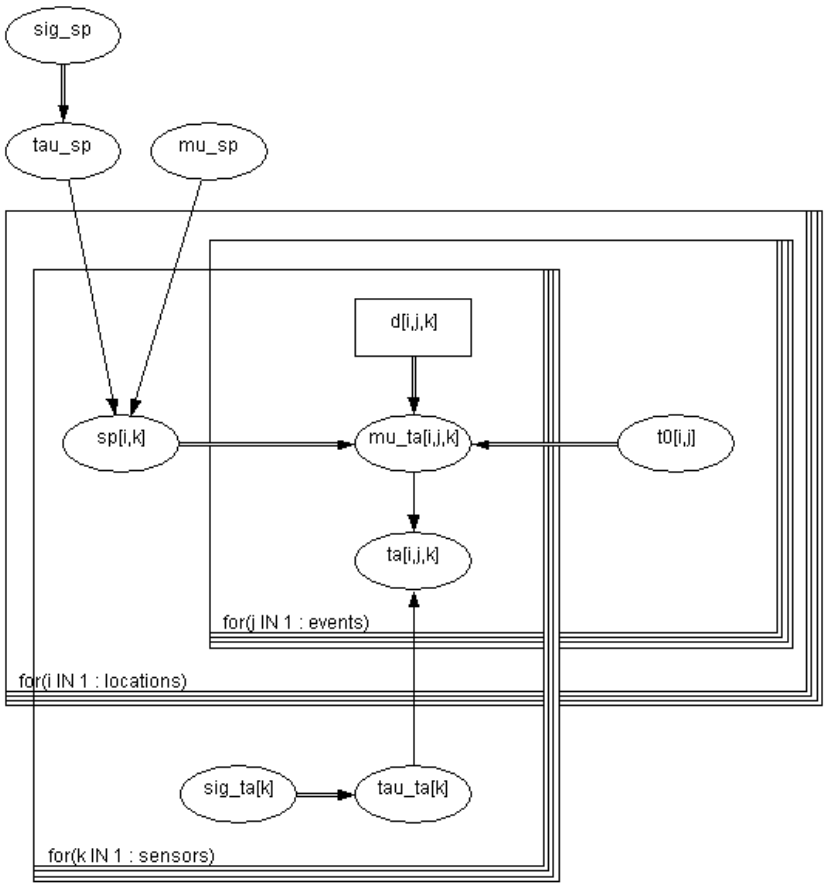

Fig. 4.7–Graphical representation of inference model (screenshot from *WinBUGS*)

Table 4.3–Description of nodes used in inference model

Param.	*WinBUGS*	Unit	Node type	Specified priors/Description
μ_{s_p}	mu_sp	[ms/m]	Stochastic	N(0.25, 1.0)
σ_{s_p}	sig_sp	[ms/m]	Stochastic	U(0.0, 100)
τ_{s_p}	tau_sp	[(ms/m)$^{-2}$]	Logical	$\tau_{s_p} = \sigma_{s_p}^{-2}$
$\sigma_{t_a[k]}$	sig_ta[k]	[ms]	Stochastic	U(0.0, 100)
$\tau_{t_a[k]}$	tau_ta[k]	[ms^{-2}]	Logical	$\tau_{t_a[k]} = \sigma_{t_a[k]}^{-2}$
$t_{0[i,j]}$	t0[i,j]	[ms]	Stochastic	N(-0.05, 1.0)
$s_{p[i,k]}$	sp[i,k]	[ms/m]	Stochastic	N(μ_{s_p}, τ_{s_p})
$d_{[i,j,k]}$	d[i,j,k]	[m]	Constant	Calculated from 'known' locations
$\mu_{t_a[i,j,k]}$	mu_ta[i,j,k]	[ms]	Logical	Eqn. 4.11
$t_{a[i,j,k]}$	ta[i,j,k]	[ms]	Stochastic	N($\mu_{t_a[i,j,k]}$, $\tau_{t_a[k]}$), observed

4.3.2 Estimation of Model Parameters Using Bayesian Inference

The model was implemented in *WinBUGS* as described in section 4.3.1 and the analysis run to estimate the posterior distributions of all model parameters. A summary of the results is shown in Table 4.4. Listed are sample means $\overline{x}$, standard deviations *s*, coefficients of variation $CV = s\overline{x}^{-1}$, and Monte Carlo standard error of the mean. The average *p*-wave velocity c_p (determined from node μ_{s_p} by Eqn. 4.7) was 3.89 m/ms (153 in./ms) which is physically meaningful and comparable to values found in earlier studies (Schumacher 2008). Another parameter that was observed during the simulation process was $t_{0[i,j]}$, the estimated event source times. Here as well, estimated posterior values were all feasible. Finally, *R* and *P* matrices were computed containing the correlation coefficients ρ and *p*-values, respectively, to test for correlation between sampled parameters. No significant correlation was found between any of the estimated parameters, i.e. all model parameters were essentially statistically independent. PDFs were fitted and assigned to each estimated parameter based on the highest log-likelihood value and are listed in Table 4.4. As can be seen, the mean *p*-wave slowness μ_{s_p} was found to be Normal (N), and the precisions τ_{s_p} and $\tau_{t_a[k]}$ Gamma (Gam) distributed. These posterior PDFs were used in the predictive algorithm for validation of the model and is presented in the following section.

Table 4.4–Sample statistics of estimated model parameters and fitted PDFs

Par.		Posterior sample statistics				Fitted PDFs
	Unit	$\bar{x}$	s	CV	MC error	
μ_{s_p}	[m/ms]	0.2574	0.002271	0.009	5.451E-5	N(0.2574, 193800)
τ_{s_p}	[(m/ms) $^{-2}$]	3747	371.0	0.099	2.831	Gam(102.3, 0.02729)
$\tau_{ta[1]}$	[ms^{-2}]	556800	85110	0.153	500.5	Gam(43.34, 7.783E-5)
$\tau_{ta[2]}$	[ms^{-2}]	257100	35560	0.138	229.7	Gam(52.52, 2.043E-4)
$\tau_{ta[3]}$	[ms^{-2}]	1.068E6	200100	0.187	1207	Gam(29.39, 2.752E-5)
$\tau_{ta[4]}$	[ms^{-2}]	586100	90470	0.154	558.5	Gam(45.52, 7.255E-5)
$\tau_{ta[5]}$	[ms^{-2}]	512900	76490	0.149	458.3	Gam(45.48, 8.867E-5)
$\tau_{ta[6]}$	[ms^{-2}]	584200	89790	0.154	595.9	Gam(42.8, 7.325E-5)
$\tau_{ta[7]}$	[ms^{-2}]	79270	10520	0.133	73.53	Gam(56.82, 7.168E-4)
$\tau_{ta[8]}$	[ms^{-2}]	40890	5286	0.129	31.23	Gam(59.87, 0.001464)

The number of model simulation updates was selected based on convergence criteria presented in Congdon (2003): a total of 250000 were generated of which the first 50000 samples were discarded to account for the so-called burn-in time. Of the remaining 200000 samples, every 8th sample was used, producing a final sample size of 25000 samples. This process is called thinning and ensures minimal autocorrelation, i.e. interdependency of consecutive samples.

4.3.3 Implementation of Predictive Model

Based on Eqn. 4.7, a predictive model was implemented. It was based on the same probabilistic model as presented in section 4.3.1 and is visualized in Fig. 4.8. The estimated model parameters presented in Table 4.4 were utilized as priors to estimate the source locations parameters t_0, x_0, y_0, and z_0. The priors selected for the source location parameters should be based on reasonable assumptions, i.e. the following specifications are recommended based on the present study:

- Arrival times t_0: $\mathrm{N}\left(\mu_{t_0},\ \tau_{t_0}\right)$, where μ_{t_0} and τ_{t_0} can be taken similar to the values for $t_{0[i,j]}$ obtained from the parameter estimation (see section 4.3.2)
- Spatial coordinates, x_0, y_0, and z_0: $\mathrm{U}(a,\ \mathrm{b})$, where a and b are reasonable lower and upper spatial limits depending on sensor locations and specimen geometry

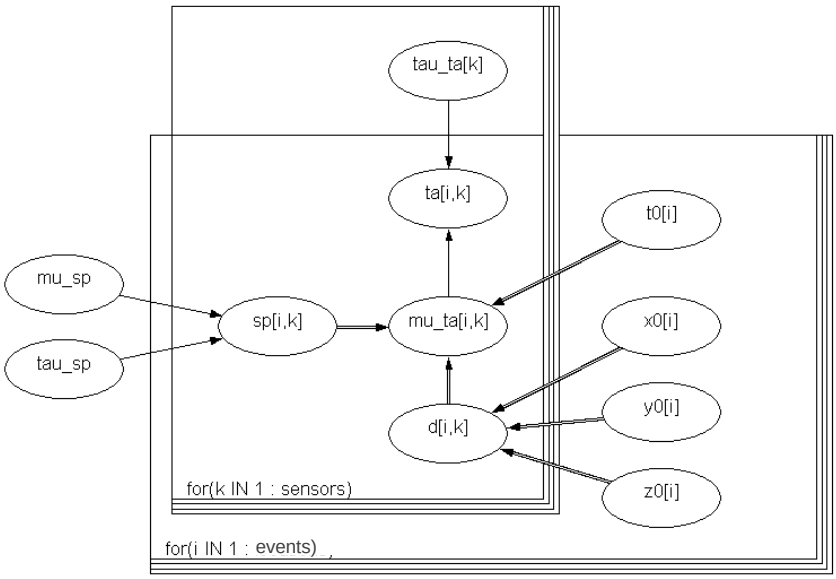

Fig. 4.8–Graphical representation of prediction model (screenshot from *WinBUGS*)

Once new time arrivals t_a are observed, the source location parameters t_0, x_0, y_0, and z_0 can be estimated using the presented predictive model. Numbers of updates were carried out following the same criteria as presented in section 4.3.2. An example of the results obtained for one event is illustrated in Fig. 4.9: all four source location parameters are available with their PDFs.

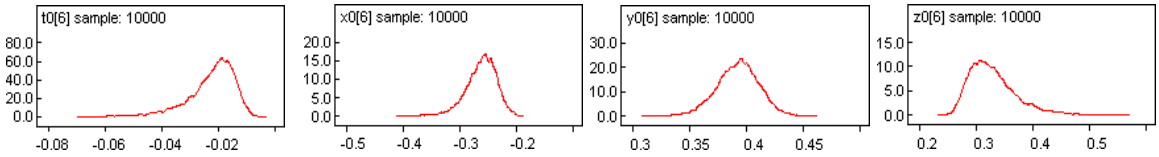

Fig. 4.9–Source location parameter results

In order to account for the three-dimensionality of the spatial part (x_0, y_0, and z_0) of the solution, an algorithm was developed that searches for the highest density within all simulated spatial points which represents the mode of the solution and therefore the point of highest probability of occurrence. This was done by dividing the three-dimensional space containing the solution 'cloud' into bins and counting the number of samples within each of those so created cubes.

The bin width h was determined based on Scott's choice (Scott 1979) and is:

$$h = \frac{8.5s}{\sqrt[3]{n}} \tag{4.13}$$

where s is the sample standard deviation and n the number of samples. A factor of 8.5 as opposed to 3.5 as suggested in the original equation was used in order to produce smoother contour plots. The mode was found as the cube with dimensions h_x, h_y, and h_z, that contained the largest number of samples (or highest density), and was represented by a white pentagram centered in that cube. The procedure to determine the three-dimensional mode was as follows:

1. Determine bin widths h for all spatial coordinates
2. Count number of samples within each cube for locations covering entire spatial data
3. Select cube containing largest number, i.e. having the highest density of samples
4. Determine spatial coordinates of that cube = mode, i.e. optimal location

The center of the cube can be highlighted if a pin-point solution for the source location is needed, e.g. when a comparison with a traditional source location algorithm is performed. In addition, two-dimensional contour plots can be generated in selected planes, e.g. the x-y plane, that pass through the mode. This was done for the same example as presented above and is shown in Fig. 4.10. The left figure shows a scatter plot of all samples in an isometric view. Sample points that lie within the slice in the x-y plane containing the highest density are shown in red. The thickness of that slice is h_z. The top-right figure represents a view on the x-y plane of the samples. The contour plot shown in the bottom-right figure was created from the points shown in red in the left and top-right figure. The center of the cube is marked with a white pentagram and represents the three-dimensional mode of the spatial coordinates x_0, y_0, and z_0.

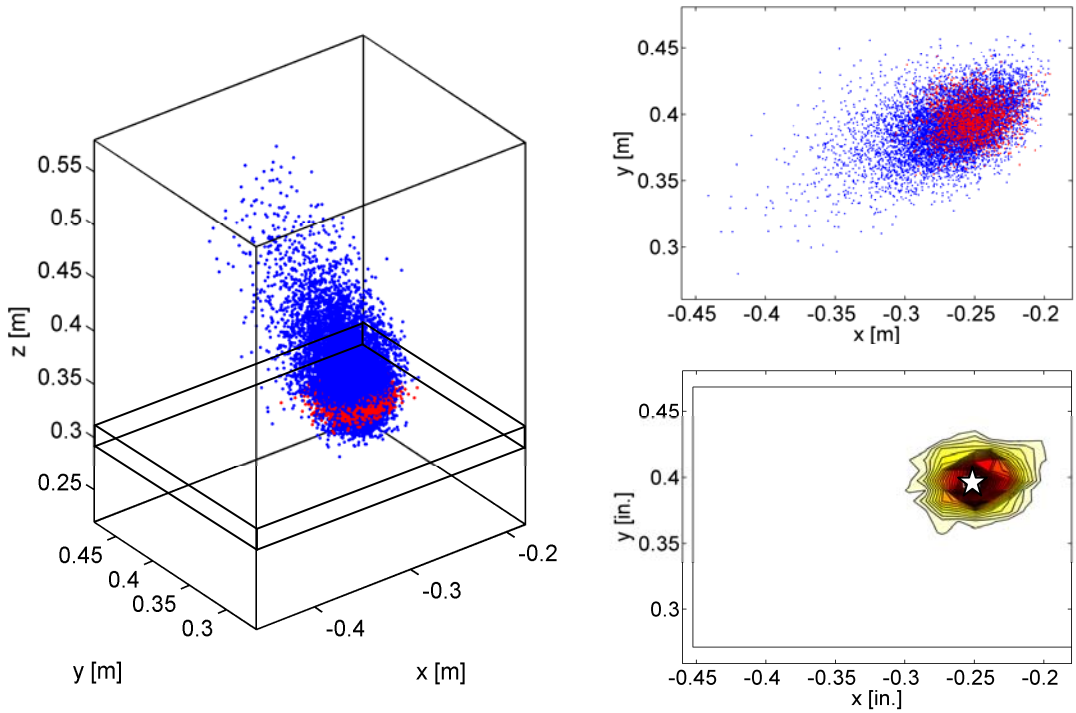

Fig. 4.10–Determination of mode of three-dimensional point 'cloud':
Left figure: Isometric view, highest density slice in *z*-direction shown in red
Top-right figure: View of *x*-*y* plane, highest density slice in *z*-direction shown in red
Bottom-right figure: Contour plot of *z*-slice with mode of highest density (spatial solution)

4.3.4 Model Validation

In order to evaluate the probabilistic model, a set of 22 PLB events on the front *x*-*y* face of the specimen that were not previously used to estimate model parameters (see section 4.3.2) were employed. The priors specified for the predictive model were: $t_0 \sim \mathrm{N}(-0.05,\ 1600)$, $x_0 \sim \mathrm{U}(-1.0,\ 1.0)$, $y_0 \sim \mathrm{U}(-0.3,\ 0.9)$, and $z_0 \sim \mathrm{U}(0.0,\ 0.6)$. The probabilistic solution is presented in Fig. 4.11. The lower-left six locations are enlarged. Scatter plots of spatial samples are shown with the contours as described in section 4.3.3 and superimposed. The coloring was removed to enhance readability. The true PLB locations are shown as blue '+'. It can be observed that the estimated mode of the solution is generally accurate for most of the PLBs. Deviations between predicted and true locations are assumed to be associated with local effects that depend on the individual signal travel path and therefore difficult to account for. Such local effects can be voids in the concrete matrix or nearby steel rebars that interfere with the propagating stress wave.

This issue could be addressed by being selective on which observed arrival times be included in the prediction, i.e. arrival times that appear to be outliers are omitted from the prediction. This could be for example done by trial and error.

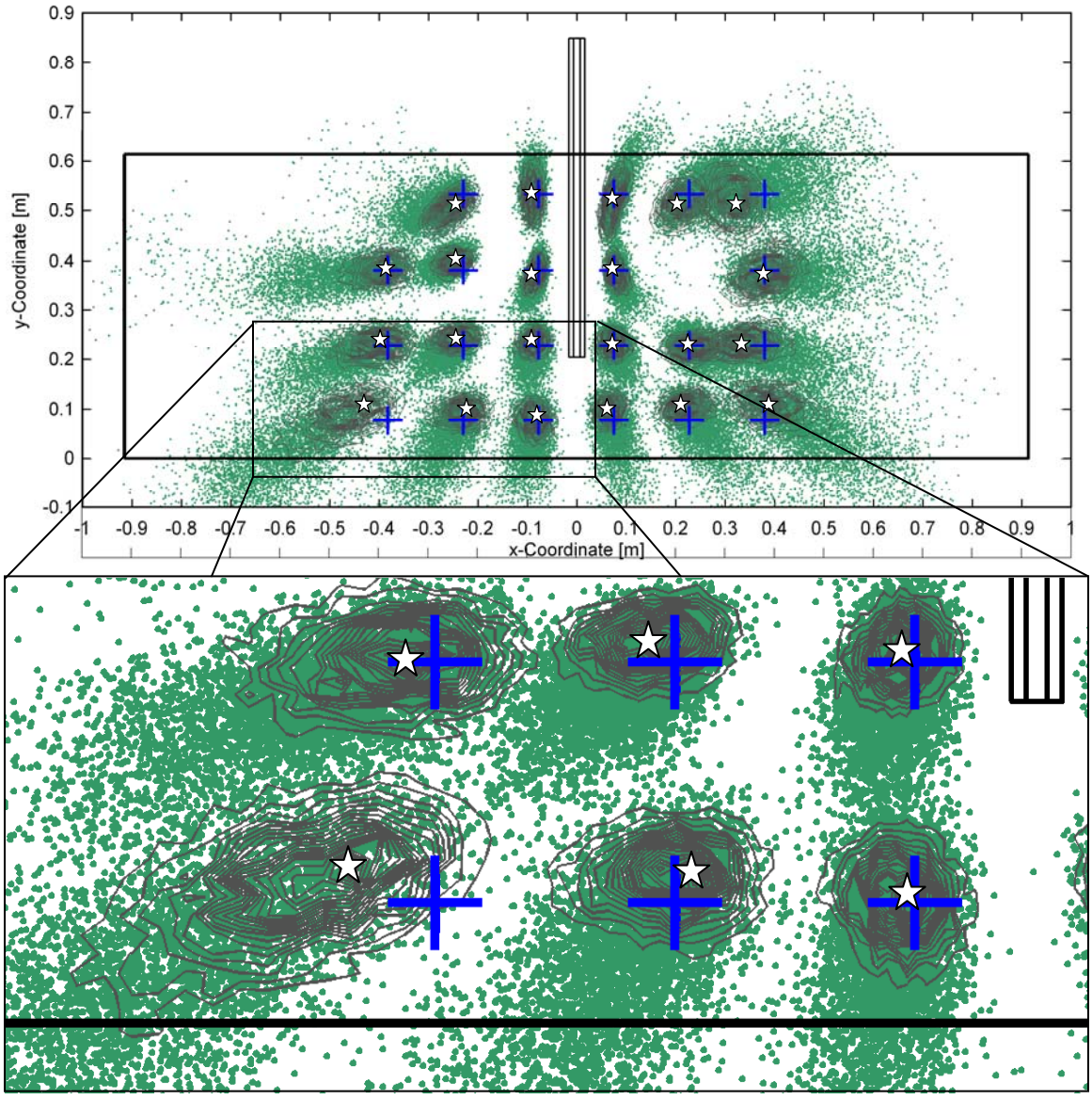

Fig. 4.11–Estimated source locations for 22 PLB events on the specimen front *x*-*y* face

4.4 Summary and Conclusions

A novel framework for the development of a probabilistic algorithm to estimate stress wave (or AE) source locations is presented. Bayesian analysis methods in conjunction with Markov Chain Monte Carlo simulation were employed to first estimate model parameters using observed data from an experiment, and then to predict source location parameters of future observations in probabilistic form. The probabilistic model that was implemented accounts for variability in the wave propagation characteristics, the measured arrival times, and the event time. Bayesian inference was found to be a powerful and flexible method to estimate parameters based on a large amount of observed data. All distribution and other parameters are estimated with their full posterior probability distributions. It was shown that predictions based on estimated parameters employing newly observed arrival times can be performed and produce accurate results. Temporal and spatial source location parameters are available in full probabilistic form as PDFs and the mode can be used as optimal location result. Extension of the presented probabilistic model by including a correction term to account for measurement uncertainty is possible and may enhance the prediction.

Future work may include the following:

- Extension of the model by including a correction term to account for measurement uncertainty employing additional observable information such as signal strength or stress wave incident angle
- Sensitivity study on model parameters, establish a ranking of the importance of each used parameter
- Comparison with traditional deterministic algorithm
- Normalization of posterior source location PDFs to obtain actual probabilities
- Evaluation of algorithm employing field data from real structures

4.5 References

Congdon, P. (2003). *Applied Bayesian Modelling*, John Wiley & Sons Ltd., West Sussex, England.

DerKiureghian, A. (2001). "Analysis of Structural Reliability under Model and Statistical Uncertainties: a Bayesian Approach." *Computational Structural Engineering*, 1(2), 81-87.

EN. (2000). "1330-9: Non-destructive testing-Terminology-Part 9: Terms used in acoustic emission testing." European Committee for Standardization (CEN), Brüssel, Belgium.

Ge, M. (2003a). "Analysis of Source Location Algorithms, Part I: Overview and non-iterative methods." *Journal of Acoustic Emission*, 21, 14-28.

Ge, M. (2003b). "Analysis of Source Location Algorithms, Part II: Iterative methods." *Journal of Acoustic Emission*, 21, 29-51.

Geiger, L. (1910). "Herdbestimmung bei Erdbeben aus den Ankunftszeiten." *Nachrichten von der Königlichen Gesellschaft der Wissenschaften zu Göttingen*, 4, 331-349.

Gilks, W. R., Richardson, S., and Spiegelhalter, D. J. (1996). *Markov Chain Monte Carlo in Practice - Interdisciplinary Statistics*, Chapman & Hall/CRC, Boca Raton, FL.

Graff, K. F. (1991). *Wave Motion in Elastic Solids*, Dover Publications, Inc., New York, NY.

Grosse, C. U., and Ohtsu, M. (2008). *Acoustic Emission Testing - Basics for Research-Applications in Civil Engineering*, Springer Verlag, Berlin & Heidelberg, Germany.

Imperial College, and Medical Research Council. (2007). "The BUGS Projedt - WinBUGS." MRC Biostatistics, Cambridge, UK, http://www.mrc-bsu.cam.ac.uk/bugs/winbugs/contents.shtml.

Koester, C. C. (2007). "Testing and Evaluation of Flexural Reinforcing Bar Anchorages Terminating in Columns," M.S. Thesis, Oregon State University, Corvallis, OR.

Kurz, J. H., Grosse, C. U., and Reinhardt, H.-W. (2005). "Strategies for reliable automatic onset time picking of acoustic emissions and of ultrasonic signals in concrete." *Ultrasonics*, 43(7), 538-546.

Lomax, A. (2008). "The NonLinLoc Software Guide." ALomax Scientific, Mouans-Sartoux, France, http://alomax.free.fr/nlloc/.

Lomax, A., Virieux, J., Volant, P., and Berge-Thierry, C. (2000). "Probabilistic Earthquake Location in 3D Layered Models." Advances in Seismic Event Location, C. H. Thurber and N. Rabinowitz, eds., Kluwer Academic Publishers, Dordrecht, The Netherlands, 101-134.

Schechinger, B. (2006). "Schallemissionsanalyse zur Ueberwachung der Schädigung von Stahlbeton," PhD Dissertation, Eidgenössische Technische Hochschule Zürich, Zurich, Switzerland.

Schumacher, T. (2006). "Acoustic Emission Monitoring of Flexural Tension Reinforcement Anchorage Zones in Full-Scale Bridge Bent Caps," M.S. Project Report, Oregon State University, Corvallis, OR.

Schumacher, T. (2008). "Acoustic Emission Techniques Applied to Conventionally Reinforced Concrete Bridge Girders." Oregon Department of Transportation (ODOT), Salem, OR.

Scott, D. W. (1979). "On optimal and data-based histograms " *Biometrika*, 66(3), 605-610.

Tarantola, A., and Valette, B. (1982). "Inverse Problems = Quest for Information." *Journal of Geophysics*, 50, 159-170.

Weber, Z. (2006). "Probabilistic local waveform inversion for moment tensor and hypocentral location." *Geophysical Journal International*, 165(2), 607-621.

5 General Conclusion

Non-destructive testing methods and applications have become of increasing interest due to the worldwide aging and deteriorating infrastructure network. Acoustic Emission (AE) monitoring in particular has its merits as it allows observing infrastructure components in real-time and detecting sudden changes in the integrity. Three manuscripts have been compiled and are included in this dissertation. The range of applications is manifold and through this dissertation, new territories have been explored that have traditionally not been part of AE research. Each one addresses pressing problems in infrastructure monitoring. The goal of the author was to cover practical as well as theoretical aspects and problems of AE monitoring in Civil Engineering and thereby push innovation.

In the first manuscript, a practical tool was implemented that can reliably detect vehicles equipped with studded tires passing a bridge. The use of studded tires has become of increasing concern to transportation agencies due to the damage caused to pavements and limited funds available for repair and replacement. Currently, no tools are available to automatically detect and report vehicles with studded tires. An integrated system to detect vehicles equipped with studded tires passing over a highway bridge is proposed. Piezo-electric sensors attached to a bridge member can detect and record stress waves that are emitted when vehicles with studded tires pass over the bridge. Discrimination of these stress waves is possible because they were found to significantly differ from stress waves caused by trucks and vehicles that have no studded tires, and from structural response. A simplified single-channel system could be practicably deployed for detection and reporting and would allow for collection of statistical data to better estimate pavement life and wear ratio and could therefore be utilized to improve design and maintenance of road surfaces. The system could further be extended for use as an enforcement tool of legal studded tire operating dates. This manuscript titled “Detection of Vehicles with Studded Tires Using Acoustic Emission Sensors Mounted to Highway Bridges” was submitted to the *ASCE Journal of Transportation Engineering* and accepted for publication on April 4, 2009.

The second manuscript titled “Estimating Operating Load Conditions on Reinforced Concrete Highway Bridges with *b*-Value Analysis from Acoustic Emission Monitoring” introduces methods to monitor and analyze bridge girders under in-service conditions. A well-known relationship between the frequency of occurrence of earthquakes and their magnitudes was

applied to AE data recorded during testing of two full-scale reinforced concrete (RC) bridge girders to evaluate load conditions of full-scale reinforced concrete bridge girders. A sophisticated experimental test setup and loading protocol accounted for realistic loading conditions including simulation of ambient traffic. It was found that the main advantage lies in real-time monitoring where for example loads that are significantly higher than experienced previous loads produce a considerable drop in the *b*-value. The proposed complementary method called *Minimum b-Value Analysis* has the potential to help estimating the operating load conditions of RC bridge girders as loads with different magnitudes produce distinguishably different *b*-value responses even under service-level loads. The AE characterizing loading can be applied using heavily loaded standard maintenance trucks that are available to most departments of transportation as was done for the presented in-service load test. The influence of factors that can affect the so-called *b*-value estimations such as stage of deterioration or external sources was studied and is introduced. This manuscript was submitted to the journal of *Structural Health Monitoring* and accepted for publication on October 5, 2009.

A novel framework for the estimation of AE source locations is introduced in the third manuscript titled “Estimation of Acoustic Emission Source Locations: A Bayesian Approach” and will be submitted to the *Journal of Sound and Vibration*. Bayesian analysis methods in conjunction with Markov Chain Monte Carlo simulation were employed to first estimate model parameters using observed data from an experiment, and then to predict source location parameters of new observations in probabilistic form. The probabilistic model that was implemented accounts for variability in the wave propagation characteristics, the measured arrival times, and the event time. Bayesian inference was found to be a powerful and flexible method to estimate parameters based on a large amount of observed data. All distribution and other parameters are estimated with their full posterior probability distributions. It was proven that location predictions based on estimated parameters employing newly observed arrival times can be performed and produce accurate results. Temporal as well as spatial source location parameters are available in full probabilistic form as PDFs and the mode can be used as optimal location result. Extension of the presented probabilistic model by including a correction term to account for measurement uncertainty is possible and may enhance the prediction. This is planned for future work.

BIBLIOGRAPHY

Angerinos, M. J., Mahoney, J. P., Moore, R. L., and O'Brien, A. J. (1999). "A Synthesis on Studded Tires." Washington State Transportation Center (TRAC), Olympia, WA.

Brunette, B. E., and Lundy, J. R. (1996). "Use and Effect of Studded Tires on Oregon Pavements." Transportation Research Record, National Academy Press, Washington, D.C., 64-72.

Carpinteri, A., Lacidogna, G., and Niccolini, G. (2006). "Critical Behaviour in Concrete Structures and Damage Localization by Acoustic Emission." *Key Engineering Materials*, 312, 305-310.

Carpinteri, A., Lacidogna, G., and Puzzi, S. (2009). "From criticality to final collapse: Evolution of the “b-value” from 1.5 to 1.0." *Chaos, Solitons & Fractals*, 41(2), 843-853.

Colombo, S. Forde, M. C., Main, I. G., and Halliday, J. (2003a). "AE monitoring of cncrete bridge beams in situ." *The Structural Engineer*, 81(23), 41-46.

Colombo, S., Main, I. G., and Forde, M. C. (2003b). "Assessing Damage of Reinforced Concrete Beam Using "b-value" Analysis of Acoustic Emission Signals." *ASCE Journal of Materials in Civil Engineering*, 15(3), 280-286.

Congdon, P. (2003). *Applied Bayesian Modelling*, John Wiley & Sons Ltd., West Sussex, England.

Cox, S. J. D., and Meredith, P. G. (1993). "Microcrack Formation and Material Softening in Rock Measured by Monitoring Acoustic Emissions." *International Journal of Rock Mechanics and Mining Sciences & Geomechanics Abstracts*, 30(1), 11-24.

DerKiureghian, A. (2001). "Analysis of Structural Reliability under Model and Statistical Uncertainties: a Bayesian Approach." *Computational Structural Engineering*, 1(2), 81-87.

EN. (2000). "1330-9: Non-destructive testing-Terminology-Part 9: Terms used in acoustic emission testing." European Committee for Standardization (CEN), Brüssel, Belgium.

Fowler, T. J., Blessing, J. A., and Conlisk, P. J. (1989). "New Directions in Testing." Third International Symposium on Acoustic Emission from Composite Materials AECM-3, Paris, France, 16-27.

Ge, M. (2003a). "Analysis of Source Location Algorithms, Part I: Overview and non-iterative methods." *Journal of Acoustic Emission*, 21, 14-28.

Ge, M. (2003b). "Analysis of Source Location Algorithms, Part II: Iterative methods." *Journal of Acoustic Emission*, 21, 29-51.

Geiger, L. (1910). "Herdbestimmung bei Erdbeben aus den Ankunftszeiten." *Nachrichten von der Königlichen Gesellschaft der Wissenschaften zu Göttingen*, 4, 331-349.

Gilks, W. R., Richardson, S., and Spiegelhalter, D. J. (1996). *Markov Chain Monte Carlo in Practice - Interdisciplinary Statistics*, Chapman & Hall/CRC, Boca Raton, FL.

Glaser, S. D. (2004). "Some Real-World Applications of Wireless Sensor Nodes." SPIE Smart Structures and Materials 2004, San Diego, CA, 344-355.

Graff, K. F. (1991). *Wave Motion in Elastic Solids*, Dover Publications, Inc., New York, NY.

Grosse, C. U. (1996). "Quantitative zerstörungsfreie Prüfung von Baustoffen mittels Schallemissionsanalyse und Ultraschall," PhD Dissertation, University of Stuttgart, Stuttgart, Germany.

Grosse, C. U., Glaser, S. D., and Krüger, M. (2006). "Condition Monitoring of Concrete Structures Using Wireless Sensor Networks and MEMS." SPIE Smart Structures and

Materials: Sensors and Smart Structures Technology for Civil, Mechanical, and Aerospace Systems, 407-418.

Grosse, C. U., and Ohtsu, M. (2008). *Acoustic Emission Testing - Basics for Research-Applications in Civil Engineering*, Springer Verlag, Berlin & Heidelberg, Germany.

Grosse, C. U., Reinhardt, H.-W., and Dahm, T. (1997). "Localization and classification of fracture types in concrete with quantitative acoustic emission measurement techniques." *NDT & E International*, 30(4), 223-230.

Grosse, C. U., Reinhardt, H.-W., and Finck, F. (2003). "Signal-Based Acoustic Emission Techniques." *ASCE Journal of Materials in Civil Engineering*, 15(3), 274-279.

Gutenberg, B., and Richter, C. F. (1949). *Seismicity of the earth and associated phenomena*, Princeton University Press, Princeton, NJ.

Hardy, H. R., Jr. (1971). "Application of Acoustic Emission Techniques to Rock Mechanics Research." Symposium on Acoustic Emission at the ASTM Committee Meeting, Bal Harbor, FL.

Higgins, C. C., Miller, T. H., Rosowsky, D. V., Yim, S. C., Potisuk, T., Daniels, T. K., Nicholas, B. S., Robelo, M. J., Lee, A.-Y., and Forrest, R. W. (2004a). "Assessment Methodology for Diagonally Cracked Reinforced Concrete Deck Girders." Oregon Department of Transportation (ODOT), Salem, OR.

Higgins, C. C., Yim, S. C., Miller, T. H., Robelo, M. J., and Potisuk, T. (2004b). "Remaining Life of Reinforced Concrete Beams with Diagonal-Tension Cracks." Oregon Department of Transportation (ODOT), Salem, OR.

Imperial College, and Medical Research Council. (2007). "The BUGS Projedt - WinBUGS." MRC Biostatistics, Cambridge, UK, http://www.mrc-bsu.cam.ac.uk/bugs/winbugs/contents.shtml.

Kaiser, J. (1950). "Untersuchungen über das Auftreten von Geräuschen beim Zugversuch," PhD Dissertation, Technische Universität München, Munich, Germany.

Katsaga, T., Sherwood, E. G., Collins, M. P., and Young, R. P. (2007). "Acoustic emission imaging of shear failure in large reinforced concrete structures." *International Journal of Fracture*, 148(1), 29-45.

Kobayashi, A. S., Hawkings, N. M., Chan, Y.-L., and Lin, I.-J. (1980). "A Feasibility Study of Detecting Reinforcing-Bar Debonding by Acoustic-emission Technique." *Experimental Mechanics*, 20(9), 301-308.

Köppel, S. (2002). "Schallemissionsanalyse zur Untersuchung von Stahlbetontragwerken," PhD Dissertation, Eidgenössische Technische Hochschule Zürich, Zurich, Switzerland.

Köppel, S., and Vogel, T. (2000). "Schallemissionsmessungen bei Versuchen an Stahlbeton." Institut für Baustatik und Konstruktion, Zurich, Switzerland.

Koester, C. C. (2007). "Testing and Evaluation of Flexural Reinforcing Bar Anchorages Terminating in Columns," M.S. Thesis, Oregon State University, Corvallis, OR.

Kuennen, T. (2006). "Taming Oregon's Cracked Bridges." Better Roads, Randall-Reilly Publishing Co., Des Plaines, IL, 54-63.

Kurz, J. H., Grosse, C. U., and Reinhardt, H.-W. (2005). "Strategies for reliable automatic onset time picking of acoustic emissions and of ultrasonic signals in concrete." *Ultrasonics*, 43(7), 538-546.

Kurz, J. H., Finck, F., Grosse, C. U., and Reinhardt, H.-W. (2006). "Stress Drop and Stress Redistribution in Concrete Quantified Over Time by the b-value Analysis." *Structural Health Monitoring*, 5(1), 69-81.

Landis, E. N., and Shah, S. P. (1995). "Frequency-Dependent Stress Wave Attenuation in Cement-Based Materials." *ASCE Journal of Engineering Mechanics*, 121(6), 737-743.

Lomax, A. (2008). "The NonLinLoc Software Guide." ALomax Scientific, Mouans-Sartoux, France, http://alomax.free.fr/nlloc/.

Lomax, A., Virieux, J., Volant, P., and Berge-Thierry, C. (2000). "Probabilistic Earthquake Location in 3D Layered Models." Advances in Seismic Event Location, C. H. Thurber and N. Rabinowitz, eds., Kluwer Academic Publishers, Dordrecht, The Netherlands, 101-134.

Lovejoy, S. C. (2006). "Development of coustic Emissions Testing Procedures Applicable to Convetionally Reinforced Concrete Deck Girder Bridges Subjected to Diagonal Tension Cracking," PhD Dissertation, Oregon State University, Corvallis, OR.

Lovejoy, S. C. (2008). "Acoustic Emission Testing of Beams to Simulate SHM of Vintage Reinforced Concrete Deck Girder Highway Bridges." *Structural Health Monitoring*, 7(4), 329-346.

Malik, M. G. (2000). "Studded Tires in Oregon-Analysis and Pavement Wear and Cost of Mitigation." Oregon Department of Transportation, Salem, OR.

Miller, R. K., Hill, E. v. K., and Moore, P. O. (2005). *Nondestructive Testing Handbook - Volume 6 - Acoustic Emission Testing*, American Society for Nondestructive Testing (ASNT), Columbus, OH.

Ohtsu, M. (1996). "The history and development of acoustic emission in concrete engineering." *Magazine of Concrete Research*, 48(177), 321-330.

Ohtsu, M., Okamoto, T., and Yuyama, S. (1998). "Moment Tensor Analysis of Acoustie Emission for Cracking Mechanisms in Concrete." *ACI Structural Journal*, 95(2), 87-95.

Ohtsu, M., Uchida, M., Okamoto, T., and Yuyama, S. (2002). "Damage Assessment of Reinforced Concrete Beams Qualified by Acoustic Emission." *ACI Structural Journal*, 99(4), 411-417.

Pollock, A. A. (1981). "Acoustic Emission Amplitude Distributions." International Advances in Nondestructive Testing, 215-239.

Potisuk, T., and Higgins, C. C. (2007). "Field Testing and Analysis of CRC Deck Girder Bridges." *ASCE Journal of Bridge Engineering*, 12(1), 53-63.

Rao, M. V. M. S., and Prasanna Lakshmi, K. J. (2005). "Analysis of b-value and improved b-value of acoustic emissions accompanying rock fracture." *Current Science*, 89(9), 1577-1582.

Rundle, J. B., Turcotte, D. L., Shcherbakov, R., Klein, W., and Sammis, C. (2003). "Statistical Physics Approach to Understanding the Multiscale Dynamics of Earthquake Fault Systems." *Reviews of Geophysics*, 41(4), 5.1-5.30.

Schechinger, B. (2006). "Schallemissionsanalyse zur Ueberwachung der Schädigung von Stahlbeton," PhD Dissertation, Eidgenössische Technische Hochschule Zürich, Zurich, Switzerland.

Schumacher, T. (2006). "Acoustic Emission Monitoring of Flexural Tension Reinforcement Anchorage Zones in Full-Scale Bridge Bent Caps," M.S. Project Report, Oregon State University, Corvallis, OR.

Schumacher, T. (2008). "Acoustic Emission Techniques Applied to Conventionally Reinforced Concrete Bridge Girders." Oregon Department of Transportation (ODOT), Salem, OR.

Schumacher, T., Higgins, C. C., and Lovejoy, S. C. (2009). "Detection of Studded Tires Using Acoustic Emission Sensors Mounted to Highway Bridges." *ASCE Journal of Transportation Engineering*(accepted for publication on 04/24/2009).

Scott, D. W. (1979). "On optimal and data-based histograms " *Biometrika*, 66(3), 605-610.

Shiotani, T., and Ohtsu, M. (1998). "Prediction of Slope Failure Based on AE Activity." Acoustic Emission: Standards and Technology Update, ASTM STP 1353, American Society for Testing and Materials, 156-171.

Shiotani, T., and Ohtsu, M. (2000). "Prediction of Slope Failure Based on AE Activity." Acoustic Emission: Standards and Technology Update - ASTM STP 1353, West Conshohocken, PA, 156-171.

Shiotani, T., Yuyama, S., Li, Z. W., and Ohtsu, M. (2000). "Quantitative Evaluation of Fracture Processes in Concrete by the Use of Improved b-Value." Non-Destructive Testing in Civil Engineering 2000 (Seiken Symposium No. 26), Elsevier, Tokyo, Japan, 293-302.

Stein, S., and Wysession, M. (2003). *An Introduction to Seismology, Earthquakes, and Earth Structure*, Blackwell Publishing Ltd., Malden, MA.

Tarantola, A., and Valette, B. (1982). "Inverse Problems = Quest for Information." *Journal of Geophysics*, 50, 159-170.

Uomoto, T. (1987). "Application of Acoustic Emission to the Field of Concrete Engineering." *Journal of Acoustic Emission*, 6(3), 137-144.

Weber, Z. (2006). "Probabilistic local waveform inversion for moment tensor and hypocentral location." *Geophysical Journal International*, 165(2), 607-621.

Weiss, J. (1997). "The Role of Attenuation on Acoustic Emission Amplitude Distributions and b-Values." *Bulletin of the Seismological Society of America*, 87(5), 1362-1367.

WSDOT. (2006). "Pavements and Studded Tire Damage." Washington Department of Transportation (WSDOT)-Materials Laboratory, Olympia, WA.

Zubeck, H., Larson, E., Aleshire, L., Harvey, S., and Porhola, S. (2004). "Socio-Economic Effects of Studded Tire Use in Alaska." State of Alaska, Anchorage, AK.